BIPM Report BIPM-2000/9

REPORT

ON THE

INTERNATIONAL COMPARISON OF CRYOGENIC RADIOMETERS

BASED ON TRANSFER DETECTORS

BIPM September 2000

R. Goebel, M. Stock, R. Köhler

TABLE OF CONTENTS

Introduction

Following the decisions of the 1994 meeting of the Consultative Committee for Photometry and Radiometry (CCPR) the BIPM acted as pilot laboratory for an international comparison of cryogenic radiometers carried out using silicon trap detectors as transfer instruments [1]. The circulation of the transfer detectors started in July 1996 and ended in February 1999.

The details of the comparison were drawn up by a working group consisting of CSIRO, NIST, NPL, NRC and the BIPM.

This report describes the principles of the comparison, the preliminary measurements at the BIPM and the results obtained with the participating laboratories.

Changes made to the three Progress Reports already distributed

This report is mainly based on the three BIPM 'Progress Reports' sent after each round of the comparison. The Progress Reports were confidential and their circulation was restricted to those laboratories that had already sent in their calibration results.

Please note that some changes have been made to the results already published in these Progress Reports:

- some laboratories have performed a new series of calibrations,
- some laboratories have sent revised values after the publication of the results,
- the uncertainty of the comparison has been enlarged to take into account the long-term drifts of the transfer detectors,
- the results of the third group have been corrected for this long-term drift (see section 3.2).

In any case, both the old and the new values are presented, together with the reasons leading to the changes.

1. Organization of the comparison

1.1. Method

Most of the cryogenic radiometers available today are transportable to some extent, and some of them have already been compared directly by transporting complete systems from one laboratory to another [2, 3, 24]. This procedure is too time-consuming, however, for a large-scale international comparison. The method of an indirect comparison by means of transfer detectors [4] was therefore chosen by the CCPR, even though the uncertainty in indirect comparisons is necessarily larger (although not very much larger). An indirect comparison does have the advantage that it also provides a means of testing the capability of the participating laboratories to transfer the accuracy of their primary reference.

Trap detectors which are known for their very stable responsivity [5] were chosen as transfer instruments and the laser wavelengths listed in Table 1 were selected for the comparison. Almost all participants used laser sources, but the use of a monochromator-based system was also possible.

476.243 nm	(Krypton line)
487.986 nm	(Argon line)
514.536 nm	(Argon line), recommended common wavelength
568.188 nm	(Krypton line)
632.817 nm	(Helium-Neon line)
647.089 nm	(Krypton line)

Table 1 - Wavelengths selected for the comparison

1.2. Circulation of the detectors and time schedule

The trap detectors used in this study were constructed at the BIPM and their characteristics (responsivity, influence parameters) were carefully measured before being sent to the participating laboratories. As seventeen laboratories had agreed to take part in the comparison, it was not possible to prepare a batch of three detectors for each individual laboratory, so five batches and a number of additional reference detectors were produced. The reference detectors are identical to those sent to the participants and undergo the same measurements at all the wavelengths but are kept at the BIPM. Each participating laboratory receives two transmission traps and one reflection trap [5, 6], and is asked to calibrate the detectors using at least three wavelengths out of the list.

The comparison is organized in a modified star configuration as shown in Figure 1. Batches are calibrated at five laboratories before being returned to the BIPM where they are checked for drift. This procedure is repeated for the successive groups of five laboratories listed in Table 2. During the checks, all detectors are calibrated against the reference detectors, which are in turn regularly calibrated against the BIPM cryogenic radiometer.

The circulation of the transfer detectors followed the agreed time schedule. Only one laboratory, the NIM (China), received them but did no calibration.

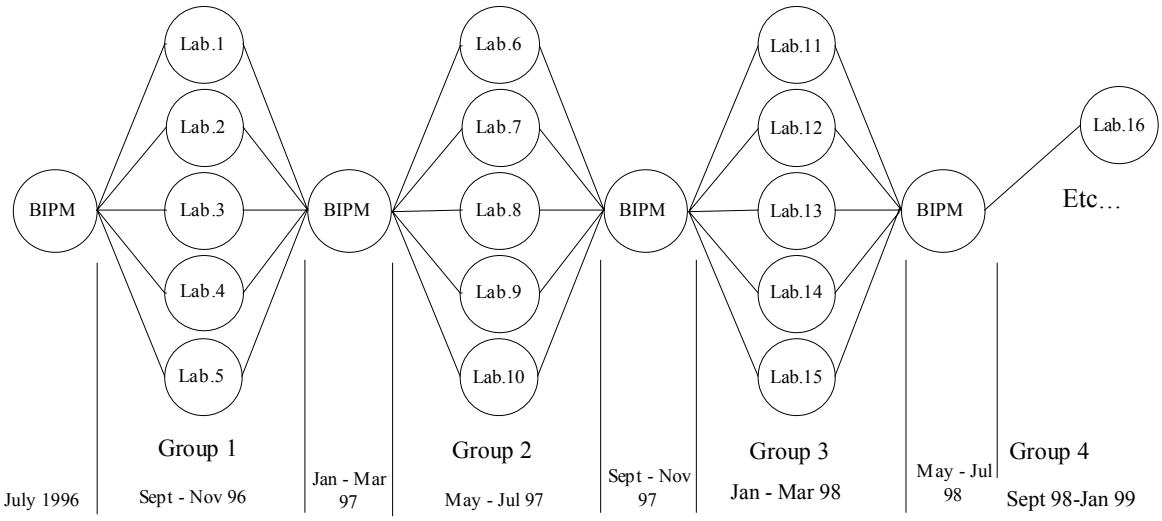

Figure 1 - Time schedule for the comparison

GROUP 1	GROUP 2	GROUP 3	GROUP 4
HUT Finland	BNM-INM France	NRC Canada	PTB -Temperature radiation Germany
NIST USA	PTB – Radiometry Germany	NMi-VSL The Netherlands	IEN Italy
NPL UK	IFA Spain	NIM China	DFM (*) Denmark
CSIRO Australia	MSL New-Zealand	ETL Japan	NIST (*) USA
SP Sweden	DFM Denmark	KRISS Korea	

Table 2 - List of participating laboratories (see list of acronyms). Laboratories marked with a (*) have also participated in a previous round.

1.3. Calculation of the relative differences

We denote by R_A the responsivity of a trap calibrated at laboratory A and by R_{BIPM} the responsivity of the same trap, calibrated at the BIPM. The relative difference Δ in the calibrations originating from the participating laboratory and the BIPM is calculated as

$$\Delta = (R_A - R_{BIPM}) / R_{BIPM} \quad . \qquad (1)$$

As all the detectors have been calibrated against the BIPM reference, which is assumed to be stable, measurements of R provided by the national laboratories can be compared to one another via this common reference.

1.4. The BIPM reference

The use of BIPM detectors linked to the BIPM cryogenic radiometer to provide a common reference does not imply R_{BIPM} is better or more accurate. It is, however, assumed to be stable: it is necessary that the reference is maintained over the whole period of the comparison with a stability compatible with the estimated uncertainties of the values of R_A being compared. The transfer detectors must also be sufficiently stable.

The stability of R_{BIPM} is assured in the following way: one batch of transmission traps and reflection traps forms a 'reference group'. Each detector of the comparison is calibrated against one trap of the reference group, which is always the same. This trap itself is regularly calibrated against the BIPM cryogenic radiometer at each of the wavelengths and compared with the other detectors of the reference group. This provides a means of comparing the behaviour of the traps that have been sent to the participating laboratories with those remaining at the BIPM, as well as providing a link to the absolute reference.

1.5. Experimental conditions

For measurements at the BIPM the following parameters were used:

beam-diameter: 2 mm to 2.5 mm ($1/e^2$ diameter)
optical power: 400 μW (typical)
temperature: 20.5 °C

Participants were not obliged to use the same values for these parameters but had to communicate the values used to the BIPM, to allow calculation of correction factors. The

use of parameters approaching those used at the BIPM should reduce the uncertainties of the comparison.

2. Preliminary measurements

It is important to determine the influence of the experimental conditions on the responsivity of the transfer detectors. This makes it possible to calculate correction factors which can be applied when comparing calibrations made under different experimental conditions, and so estimate the final uncertainty of the comparison.

2.1. Transfer detectors

Following a previous international comparison of spectral responsivity [7], the BIPM possesses a batch of fifteen three-element reflection trap detectors. Additionally, a batch of fourteen six-element transmission traps was constructed by the BIPM, following an original NIST design. Both types of trap make use of windowless Hamamatsu S1337-1010N photodiodes.

2.1.1. Spatial uniformity

The beam diameter can influence the calibration in two ways:

- the non-uniformity over the active surface of the detector can make the responsivity depend on the portion of the surface actually used, i.e. the beam size; this effect is discussed in the present section.
- at constant optical power, the irradiance is a function of the beam size, and non-linearity effects related to the use of high irradiance levels are discussed in a subsequent section.

The uniformity of the responsivity over the active surface of the detector was determined by mounting the detectors on crossed stepping motors and scanning them with a beam of about 0.5 mm diameter (see Figure 2 and Figure 3). The wavelength used was $\lambda = 514$ nm.

These data make it possible to estimate changes in responsivity as a function of spot size and alignment. To examine the effect of changing spot size, we simulated the power distribution of an approximately Gaussian beam of variable diameter. Figure 4 shows that when the beam diameter is increased from 0.5 mm to 3 mm ($1/e^2$ diameter) the response of the trap decreases by 7 parts in 10^6. A similar method can be used to simulate the influence of spatial alignment.

The beam sizes used by the participants ranged approximately from 1 mm to 2.5 mm. The effect on the responsivity was found to be small enough to be neglected when results from the BIPM were compared with those from other laboratories. However, the use of a smaller beam diameter can result in a response which depends strongly on position and non-linearity.

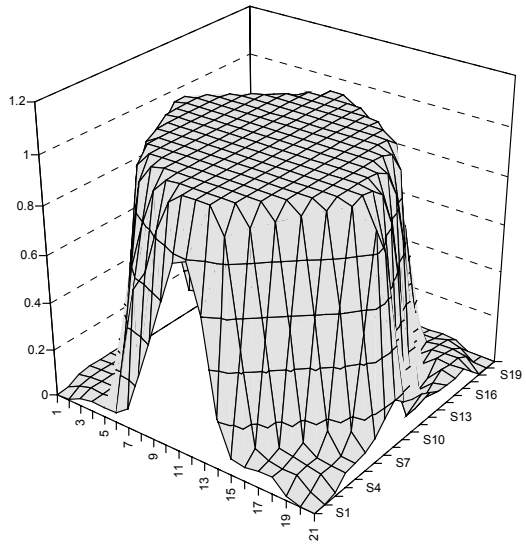

Figure 2 - Three-dimensional view: uniformity of the responsivity of a transmission trap at $\lambda = 514$ nm, normalized to unity. The scanned area is 10 mm by 10 mm.

Only a few traps were scanned with a resolution of 0.5 mm but *all* were scanned at $\lambda = 514$ nm with a 0.5 mm beam diameter ($1/e^2$) and at 1 mm intervals. Individual uniformity maps allowed the detection of contamination or the presence of dust particles on some of the detectors. These were disassembled, cleaned and checked again.

The beam diameter used at the BIPM is about 2 mm and it can be placed at the centre of the trap to within 0.2 mm. From both simulation and experimental checks, the standard uncertainty in the trap calibration arising from spatial non-uniformity was estimated to be 0.2 parts in 10^4.

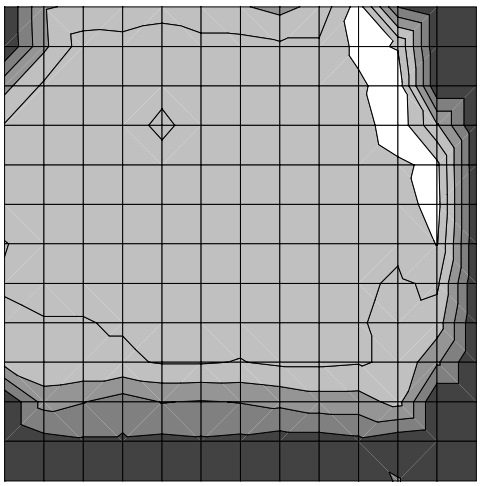

Figure 3 - Uniformity of responsivity of a transmission trap at $\lambda = 514$ nm. The scanned area is 10 mm by 10 mm. Different lines correspond to steps of 1 part in 10^4.

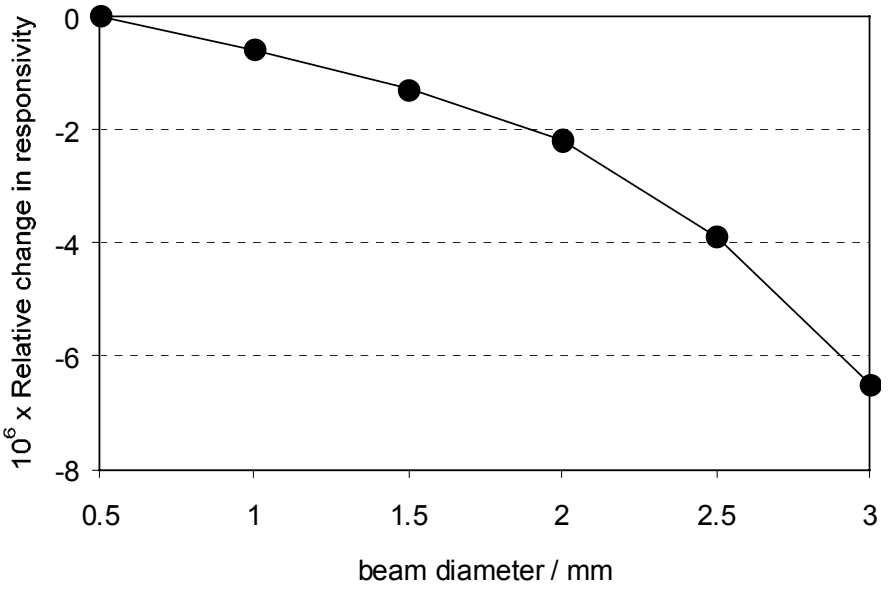

Figure 4 - Spatial uniformity effects at λ = 514 nm: relative change in responsivity of a reflection trap as a function of beam ($1/e^2$) diameter.

2.1.2. Temperature coefficient

The relative change of detector responsivity as a function of temperature was determined by placing detectors in a temperature-controlled copper housing. The temperature of the water circulating in the copper block was stabilized by means of a commercial temperature-controlled water bath. The laser beam intensity was stable to within 2 parts in 10^5 over one hour, and the temperature of the detectors was set to within 0.1°C at different steps in the range 18 °C to 25 °C.

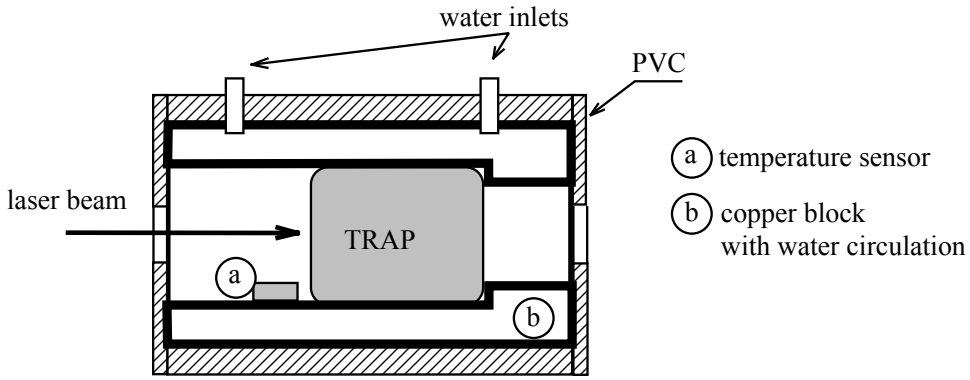

Figure 5 –Temperature-controlled housing used to measure the temperature coefficient of the trap detectors.

The temperature coefficient of the trap detectors was found to be small relative to the temperature coefficient of the single photodiodes from which they are constructed.

As the reflectance of traps and single-element photodiodes differs considerably (about 0.3% and 30% respectively), it was decided to measure the temperature dependence of the reflectance. Single photodiodes, taken from the batches used to construct the traps, were placed in the housing and inclined by 2°, so that the relative variations of the reflected beam could be recorded.

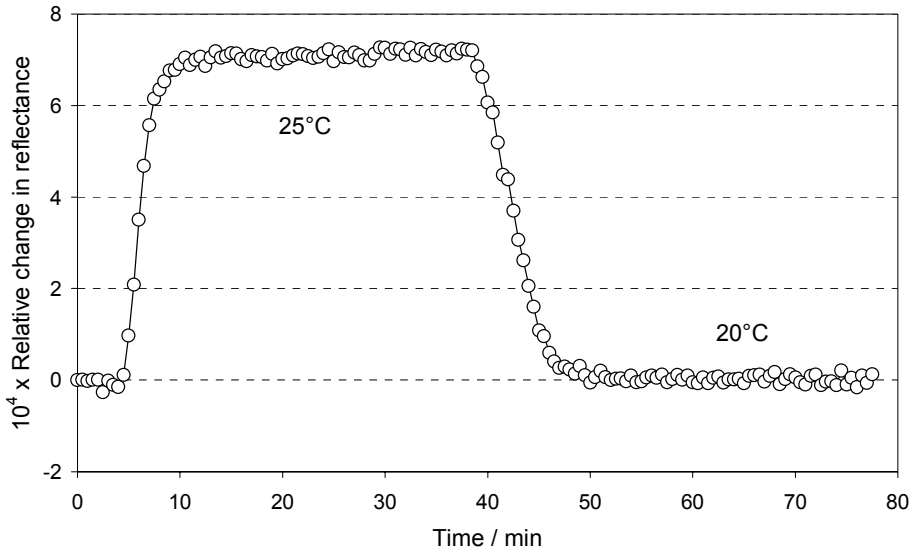

Figure 6 - Relative change in reflectance of a single photodiode as a function of temperature, at λ = 476 nm.

Results (Figure 6) show large variations of the reflectance as a function of temperature, explaining a major part of the responsivity changes. In contrast, trap detectors having a very low residual reflectance (or transmittance), are much less sensitive to these changes. Experiments made at 476 nm and 647 nm show that the trap temperature coefficient is four to five times smaller than that of single elements. Our results also showed that the temperature coefficients of photodiodes of the same type but taken from different batches, are not identical. This explains the differences found between reflection traps and transmission traps.

From earlier experiments [7, 8] it is known that the temperature coefficient varies smoothly in the visible wavelength region. The temperature coefficients were measured at 476 nm and 647 nm, and interpolated for the other wavelengths. Results are summarized in Table 3.

Traps	Wavelength / nm					
	476	488	514	568	633	647
	Temperature coefficient: / ($10^{-5} \times °C^{-1}$)					
Transmission traps	-1.5	-1.4	-1.3	-1.0	-0.6	-0.5
Reflection traps	-2.6	-2.5	-2.2	-1.7	-1.0	-0.9

Table 3 - Temperature coefficients of the transfer detectors as a function of wavelength

From Table 3, one can see that an uncertainty of 1°C in the detector temperature can contribute significantly to the total uncertainty, especially in the blue region. Moreover, large temperature differences in calibration temperatures lead to large correction factors when comparing the results from different laboratories.

At the BIPM, the temperature of a trap is measured by means of a Pt25 sensor, thermally linked to its mechanical support, with a standard uncertainty of 0.1°C.

2.1.3. Sensitivity to beam polarization

The responsivity of a good transfer detector should not depend on the polarization state of the beam to be measured. In other words, the responsivity of a trap detector aligned in a linearly polarized beam should not vary when rotated about the beam axis.

Both types of trap made at the BIPM are meant to fulfil the condition of polarization independence [6, 9, 10] which are: proper geometrical construction of the trap and similarity of all photodiodes mounted in a particular trap. However, measurements and numerical simulation [11] indicate that very small departures of the photodiodes from their ideal orientation cause a trap to show a significant sensitivity to the state of polarization of the beam. Each trap was therefore tested at $\lambda = 476$ nm, a wavelength at which the effect is known to be large. The light source was an intensity-stabilized laser producing a vertically polarized beam. The detectors were placed in the beam and then rotated around the beam axis to simulate the effect of rotation of the plane of polarization. The photoelectric signal was recorded as a function of the rotation angle and normalized to the value obtained at an arbitrarily chosen origin, to detect relative variations of responsivity (see Figure 7 and [11]). The relative variations ranged from a few parts in 10^5 up to $\pm$ 1 part in 10^4.

As a consequence, to avoid changes due to misalignment, the detectors must always be oriented the same way with respect to the direction of polarization throughout calibration and comparisons. The alignment procedure is described in the documents sent to the participants with the detectors (see Appendix).
In the worst case, an uncertainty of 2° in the orientation of the trap leads to a relative standard uncertainty of 1 part in 10^5 in the determination of the responsivity.

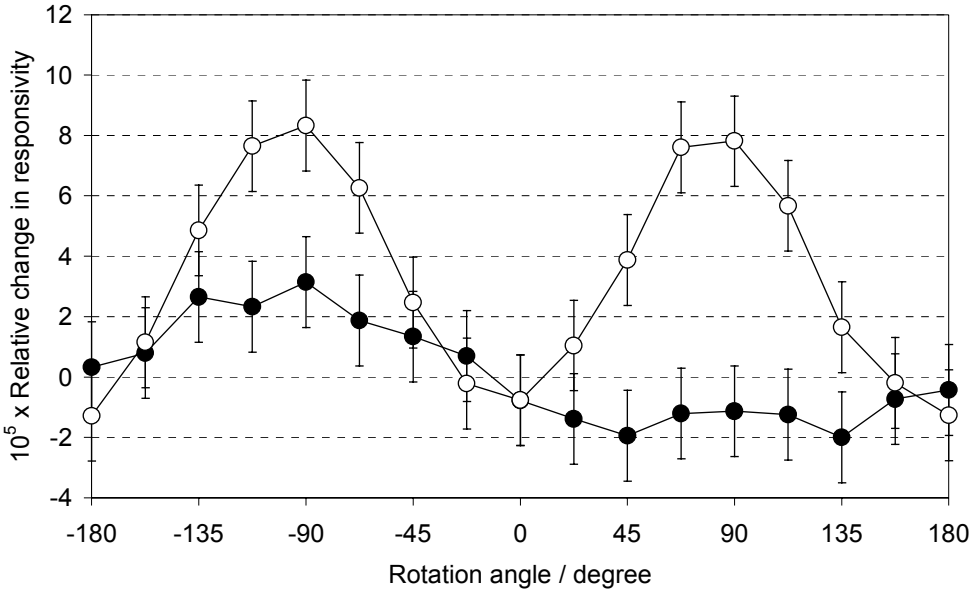

Figure 7 - Relative change in responsivity as a function of the rotation angle about the beam axis. The example shows the behaviour of two different transmission traps at $\lambda = 476$ nm.

2.1.4. Linearity

Two different experimental arrangements were used to test the linearity [8, 12, 13, 14] of the detectors. One is based on an ac technique [15], the other on classical DC flux addition [16].

2.1.4.a. AC technique

A weak modulated beam (about 20 μW) is superimposed on a dc beam whose intensity can be varied from 0 mW to 1 mW. A synchronous amplifier detects the ac signal, whose amplitude is proportional to the derivative of the curve:

$$I_{ph} = f(P_{opt})$$

where I_{ph} is the photocurrent and P_{opt} the dc incident optical power (see Figure 8)
The actual non-linearity of the detector in the range 20 μW to 1 mW is then calculated by numerical integration.
The results obtained show that:

- the non-linearities lie within the uncertainties of the measurements, 3 parts in 10^5, for optical powers below 500 μW and a beam diameter of about 2 mm ($1/e^2$), confirming that the optical parameters chosen for the comparison do not significantly increase the total uncertainties.
- the amplitude of the non-linearities depends strongly, at constant optical power, on the beam diameter (i.e. on the irradiance level).

As a conclusion of the first experiment, it became evident that the beam diameter is an important parameter. But, as at that time the BIPM had no beam analyzer, it was not possible to carry out an accurate quantitative study of this effect, especially for small beam diameters. The decision was taken, therefore, to purchase a beam analyzer and to repeat the measurements using the dc technique, both to cross-check the data and to confirm the first results.

2.1.4.b. Flux addition dc technique

The incoming beam is divided into two beams of similar power and of orthogonal polarizations A and B by means of a half-wave plate and a polarizing beam splitter (see Figure 9).

The non-linearity N is then defined as:

$$N = \frac{I_{AB}}{I_A + I_B} - 1 \qquad (2)$$

where I_A and I_B are the photocurrents measured with beams A and B respectively, and I_{AB} with both beams acting together. The non-linearity effect over a wider range is here also obtained by numerical integration.

As shown on Figure 10 and Figure 11 the new data confirm the first results.

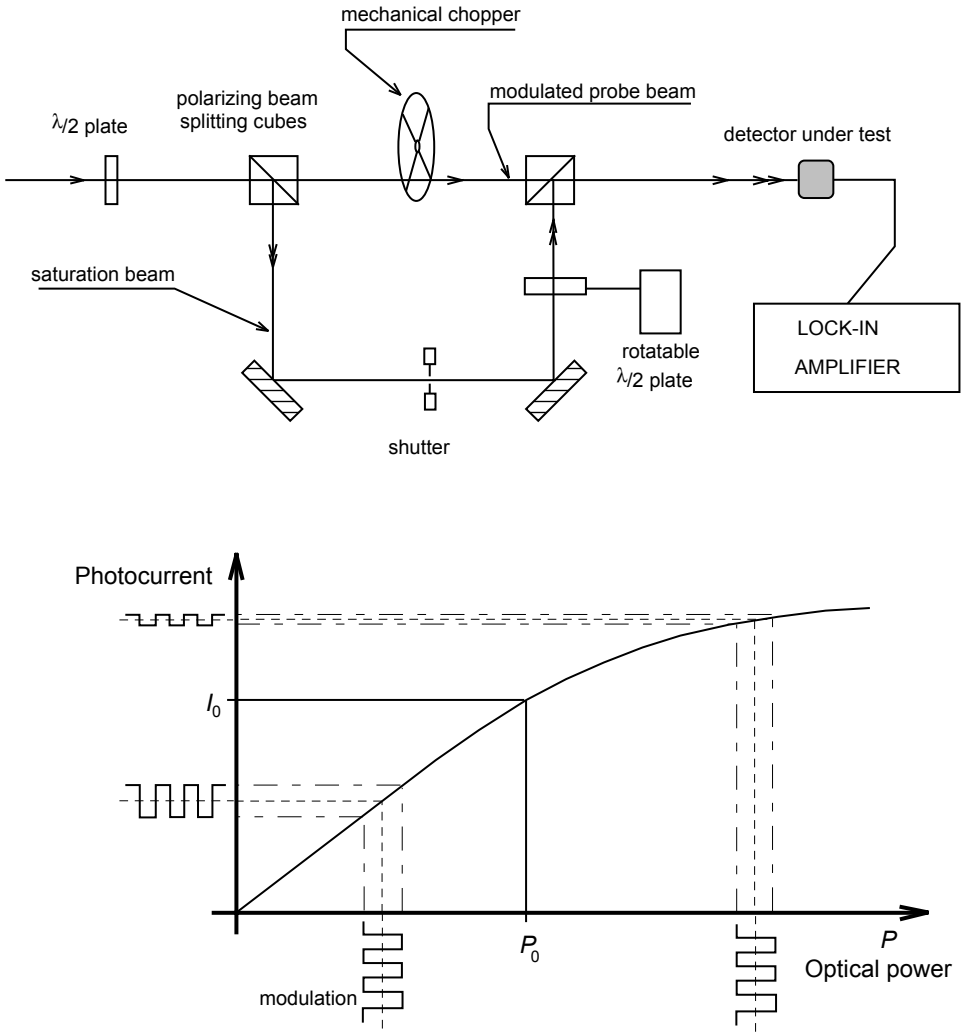

Figure 8 - Linearity measurement: principle of the ac technique.

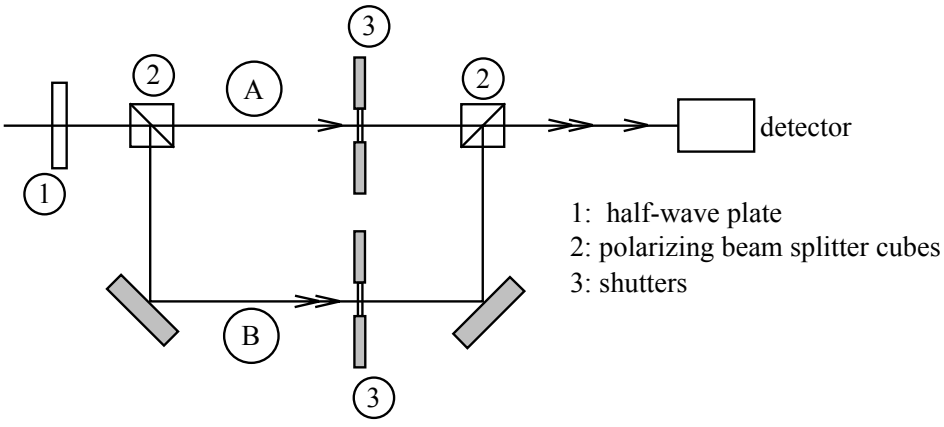

Figure 9 - Experimental arrangement used for non-linearity measurements by flux addition.

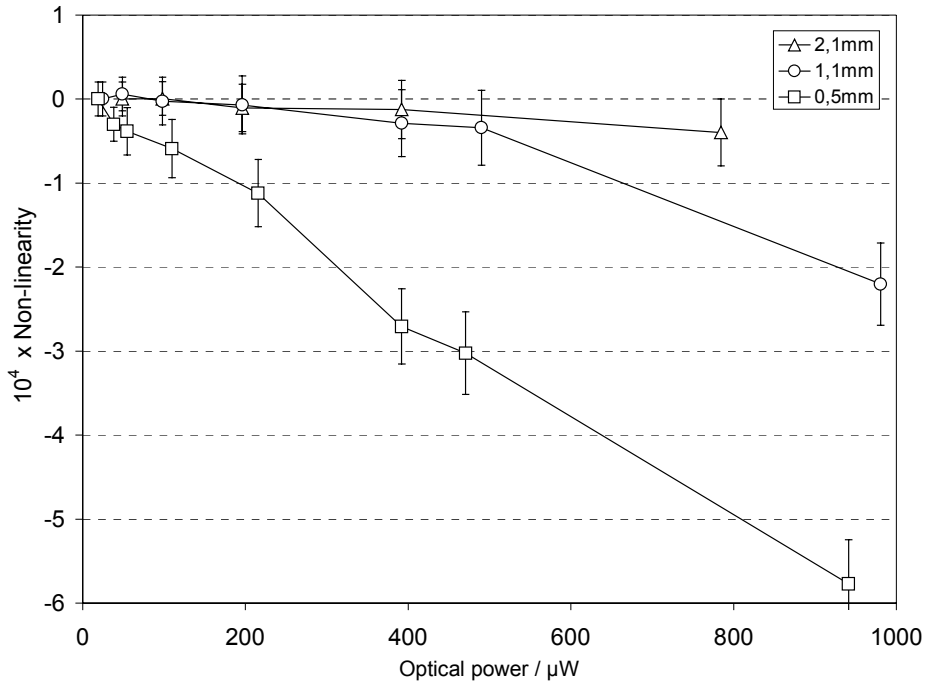

Figure 10 - Non-linearity of a reflection trap as a function of optical power for three different beam diameters ($1/e^2$) at $\lambda = 633$ nm.

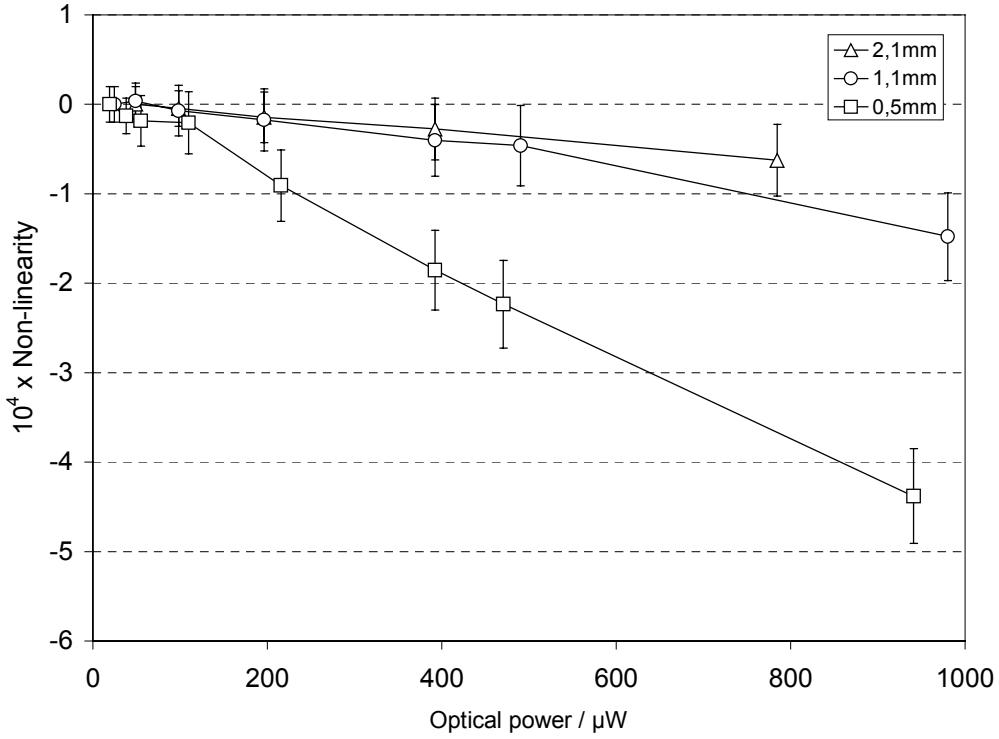

Figure 11 - Non-linearity of a transmission trap as a function of optical power for three different beam diameters ($1/e^2$ diameter) at $\lambda = 633$ nm.

The dependence of the non-linearity on both the total flux absorbed and the irradiance level can also be demonstrated by a simple experiment.

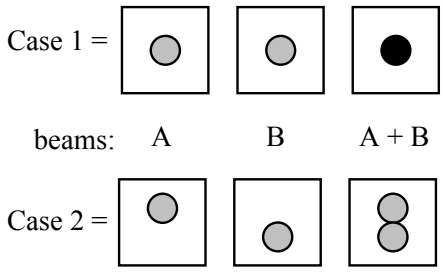

Figure 12 - Two possible alignments of beams A and B on the photodetector: superimposed (case 1) or side by side (case 2).

Figure 12 shows the positions of beams A and B on the sensitive surface of the detector:

- In case 1, they are superimposed: both the total flux and the irradiance level are doubled.
- In case 2, the optical power is doubled at constant irradiance level.

With the following experimental conditions:
beam diameters: 0.5 mm ($1/e^2$)
optical power: both beams 0.5 mW at $\lambda = 633$ nm,
the non-linearity as defined in expression (2) for a power step: 0.5 mW to 1 mW, was

$N_1 = -2.3 \times 10^{-4}$ and $N_2 = -0.5 \times 10^{-4}$ for cases 1 and 2 respectively.

This result confirms that, at optical powers around 0.5 mW, non-linearity effects are largely dominated by the irradiance level.

Conclusion: for optical powers below 0.5 mW and beam diameters not smaller than 1.1 mm, the standard uncertainty introduced by non-linearity effects was estimated to be 3 parts in 10^5 when comparing results from different laboratories. However, as non-linearity is in fact mainly related to the photocurrent density or to the total photocurrent, it would have been probably more appropriate to recommend a maximum photocurrent rather than a maximum optical power.

As non-linearity effects depend strongly on the beam diameter, and also probably on the beam shape (if not approximately Gaussian), the calculation of correction factors would be very difficult if detectors were used under conditions other than those recommended.

All the participants have followed the recommendations. They have used either:

- a beam diameter not smaller than 2 mm with an optical power below 500 μW,
- or a smaller beam diameter with reduced optical power,
- or an additional linear transfer detector.

The results have therefore not been corrected for non-linearity effects (with only one exception at one wavelength).

2.1.4.c. Induced polarization sensitivity

In a trap configuration, successive photodiodes absorb different fractions of the total power. The non-linearity induced in each photodiode is therefore different. Consequently, the photodiodes contained in a same trap can no longer be considered similar, making the detector polarization sensitive. At high irradiance level, nonlinearities cause traps to be sensitive to the polarization state of the beam, even in a trap of perfect geometry containing perfectly matched photodiodes [13].

2.1.5. Other environmental effects

From earlier measurements it is known that the influence of air humidity on trap detectors is small [17, 18] , so it is neglected here, but contamination by dust particles can cause substantial changes in responsivity. The deposition of a dust particle cannot always be avoided, even when these devices are handled carefully. Its presence can be detected either by visual inspection or by using the following procedure: the trap is slightly displaced with respect to its normal position by about 0.5 mm. The uniformity is such that the photocurrent should not change by more than 1 part in 10^4 . A larger change indicates a contamination. This can be removed by gently blowing dry air into the detector (this must be done extremely carefully).

2.2. The BIPM experimental arrangement

2.2.1. Sources

Three laser sources are used: an argon laser, a krypton laser and a helium-neon laser. The laser beam is spatially filtered and stabilized in intensity. The stability of the intensity, estimated by the standard deviation of the signal from the trap detector, is 2 parts in 10^5 over several hours. A large-area photodiode with a central hole and a beam analyzer are used to optimize the optical alignments and the beam geometry: diameter, collimation, reduction of scattered light (the BIPM experimental procedures have been described elsewhere [19, 20]).

The cryogenic radiometer is positioned in the beam using pellicle beam splitters and a high-resolution translation stage. The transfer detectors are aligned following the procedure described in the Appendix.

2.2.2. The BIPM cryogenic radiometer

The BIPM cryogenic radiometer is a commercial Radiox, from Oxford Instruments Ltd. The only significant modification made at the BIPM is to the window assembly support, a change which improves the window transmittance measurement procedure. The digital voltmeters and the standard resistor are regularly calibrated by the BIPM Electricity section. Their calibration is traceable to BIPM primary references.

3. Uncertainty budget

3.1. Repeatability of the absolute measurements

3.1.1. Short term

The short-term repeatability of responsivity measurements is usually very satisfactory (see Figure 13). In the course of a calibration series, the trap detector is pushed into the beam during the electrical substitution cycles of the radiometer. The responsivity of the trap is then calculated for each pair of measurements: photocurrent from the trap and optical power measured by the Radiox in the same beam.

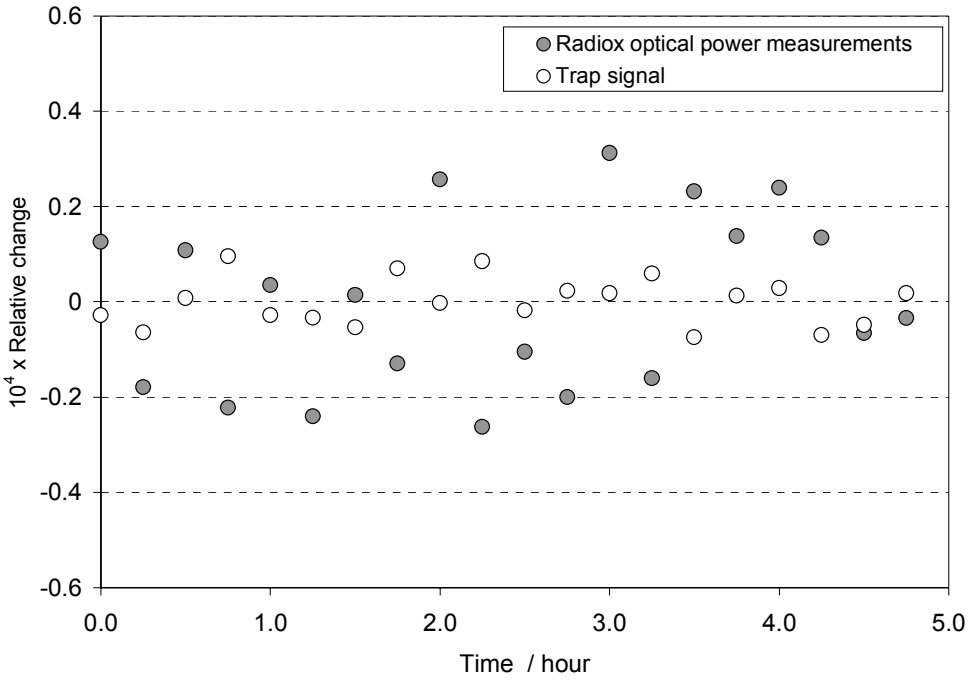

Figure 13 - Stability of the optical measurements during a calibration series at 514 nm (automated measurements performed during a single night).
Open circles: signal from the trap detector aligned in the beam.
Filled circles: optical power as measured by the cryogenic radiometer.
Relative variations are expressed in parts in 10^4

3.1.2. Long term

The long-term repeatability can be estimated from Figure 14 (open circles) which shows the relative variation of the successive calibrations of one reference trap at $\lambda = 647$ nm over more than three years (successive results are not necessarily equally spaced in time). These relative variations take into account all sources of instability over this period: detector changes, electrical calibrations, Radiox modifications, experimental conditions, etc.

The relative standard deviation is 7 parts in 10^5, which is most satisfactory, so the stability of the transfer detectors can be expected to be at least of the same order of magnitude.

Clearly this value is larger than the short-term dispersion. Beginning in 1996, the first reference detector denoted P2 (a reflection trap) has always been calibrated at the same time as another reference trap denoted T1 (a transmission trap). The relative difference ΔR of the measured responsivities was calculated as:
$\Delta R = (R_{T1} - R_{P2}) / R_{P2}$ where R_{T1} and R_{P2} are the responsivities of T1 and P2 respectively.

Variations of this ratio are plotted as filled circles on the graph. Their standard deviation is 2 parts in 10^5.
This much lower value can be explained in two ways:

- the responsivities of the two detectors vary the same way, following variations of some common influence parameter.
- the larger dispersion is introduced by long-term variations in the behaviour of the Radiox, a more probable explanation.

In any case, the uncertainty budget has to account for the global effect. The estimated type A uncertainty associated with the calibration of the transfer detectors is 7 parts in 10^5. This value includes the short-term dispersion and the noise equivalent power of the system.

As the trap to be calibrated and the absorbing cavity of the Radiox are not placed exactly at the same distance from the source, a correction factor (typical value: 0.999 98) is applied to the calibration results. An uncertainty is associated with this correction, referred to as 'distance and diameter effects' [19].

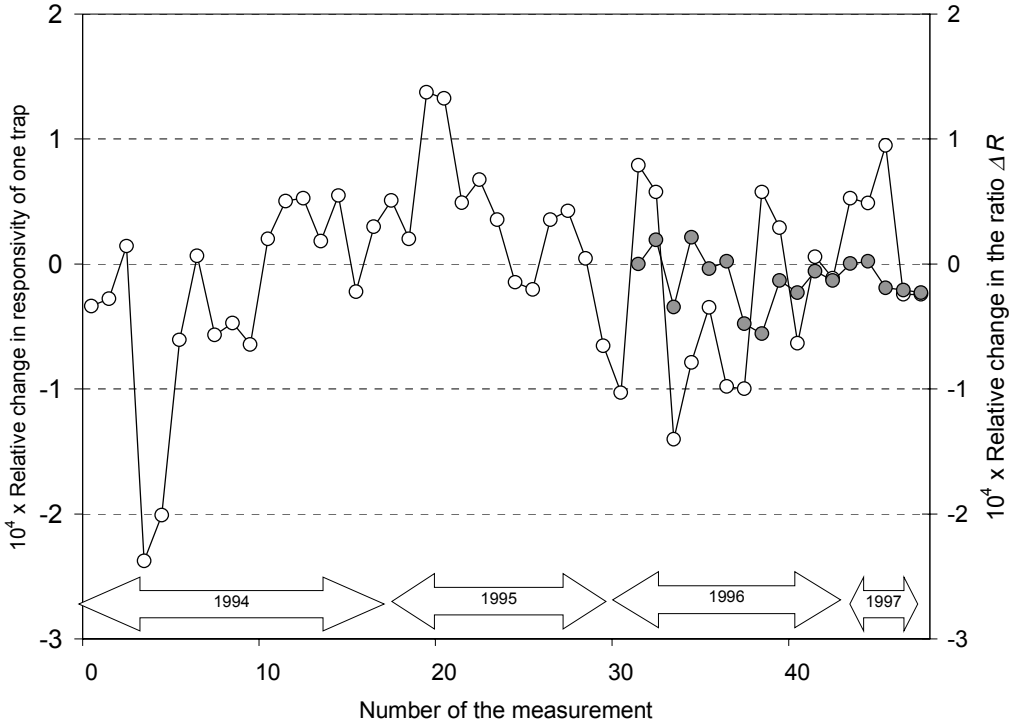

Figure 14 - Open circles: repeatability of the calibrations of a reference trap at $\lambda = 647$ nm. The trap was calibrated with the BIPM cryogenic radiometer over more than three years.
Filled circles: ratio of the responsivities of two reference traps calibrated at the same time (relative variations).

3.1.3. Transfer

It was not possible to calibrate each detector individually four times or more per wavelength against the cryogenic radiometer. This was done only for two of the reference traps, always the same pair. After calibration at each wavelength, the calibration is transferred to all the other traps by relative comparison. The transfer is made using the laser beam as it is prepared for the calibration (geometry, scattered light, power, alignment). The additional uncertainty due to this internal transfer is small (2 parts in10^5).

All these contributions are combined in the BIPM uncertainty budget, shown in Table 4.

Source of uncertainty	$10^4 \times$ relative standard uncertainty
Radiox	
Electrical power measurements	0.1
Non-equivalence electrical / optical power	0.1
Cavity absorptance	0.1
Window transmittance and scattered light	0.3
Trap detector calibration	
Spatial non-uniformity	0.2
Temperature correction	0.1
Beam polarization orientation	0.1
Linearity	0.3
Electrical calibration	0.2
Distance and diameter effects	0.1
Repeatability	0.7
Internal transfer	0.2
Relative combined standard uncertainty	**0.9**

Table 4 - BIPM uncertainty budget for the calibration of the transfer detectors used in the comparison of cryogenic radiometers.

3.2. Stability of the detectors

Previous experiments have shown that this type of trap detector is stable with time, over several months, providing it is used under controlled conditions (no dust contamination, no UV exposure nor intense irradiation). At the least, changes with time or with wavelength are likely to happen gradually and smoothly. The long-term stability of the whole group is however difficult to guarantee. In contrast, the short-term repeatability of the measurements with the cryogenic radiometer is not as good as that obtained with a group of detectors, but it can guarantee a stable long-term absolute reference.

Principle of the tests:

During the comparison, the transfer detectors are compared with the reference group of detectors so that corrections for possible changes during transport could be applied. The reference group itself is regularly calibrated against the BIPM cryogenic radiometer. If the changes in the calibration are not significantly larger than the uncertainty of the calibration (namely 1 part in 10^4), then the reference group is assumed to be stable, and no further correction is applied to the transfer detectors. If the changes are significant, one has to assume that the whole set has changed, and corrections corresponding to the new calibrations have to be applied.

3.2.1. Experimental result

After their return, the detectors are compared again with the reference group (the group remaining at the BIPM). The change of each individual detector relative to this reference group is plotted as a function of wavelength for each of the four rounds.

a) Round 1 (see Figure 15): the changes were generally smaller than 1 part in 10^4 (5 parts in 10^5 typical), showing high stability among the whole population.

b) Round 2 (see Figure 16): the changes rarely exceeded 5 parts in 10^5, confirming the high stability seen during the first round. Two exceptions must be mentioned, however. Trap T13 was contaminated by a dust particle, so that after its return

from the DFM its responsivity had decreased by more than 15 parts in 10^4. Fortunately, when the trap was irradiated with a laser beam, the particle was clearly visible on the first photodiode and was removed simply by gently blowing dry air on to it. The trap then recovered the responsivity it had had before shipment, to within a few parts in 10^5. This problem does not affect the final results because the DFM finally decided for other reasons to redo its measurements.

The other case of contamination concerned one of the reference traps kept at the BIPM, but here the particle could not be removed from the photodiode surface. The trap had to be discarded and replaced by a spare one.

This demonstrates that the contamination of the detectors is one of the major concerns in the calibration transfer. Detectors have to be kept in their protection bags when not used, but contamination is still possible during the calibration periods. Dust-free laboratories are, of course, a great advantage if available.

c) Round 3 (see Figure 17): most of the changes were not larger than 5 parts in 10^5, which is consistent with the behaviour already seen during the first two rounds.

But unexpectedly large decreases have also occurred. The responsivity of the traps T4 and P4 has decreased by 2×10^{-4} or more. They were sent to the NIM (China), where, according to the laboratory, they have not been used. No contamination by dust particles could be detected on visual inspection. The changes perhaps result from severe transport conditions; they do not depend significantly on the wavelength. In contrast, the changes in P7 sent to the KRISS are strongly wavelength dependent: a few parts in 10^5 at 647 nm, and up to 4 parts in 10^4 at 476 nm. No explanation was found for this effect, but when changes are that large, the estimated uncertainty associated with the comparison has to be increased. None of these three traps was used in the fourth round of the comparison.

d) Round 4 (see Figure 18): the relative changes of the transfer detectors when compared with the reference group are very small, within ± 5 parts in 10^{-5}. This indicates that the repeatability of the comparisons is satisfactory, even if this does not prove the stability of the whole set.

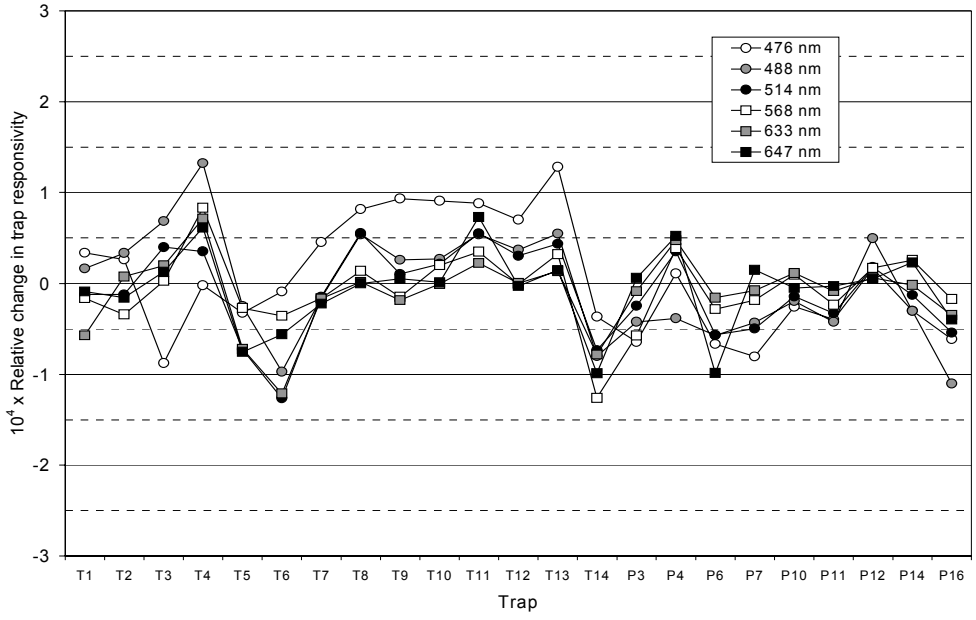

Figure 15 - Round 1. Stability of the transfer detectors when compared with the reference group: relative change in responsivity at each wavelength, as measured after return to the BIPM.

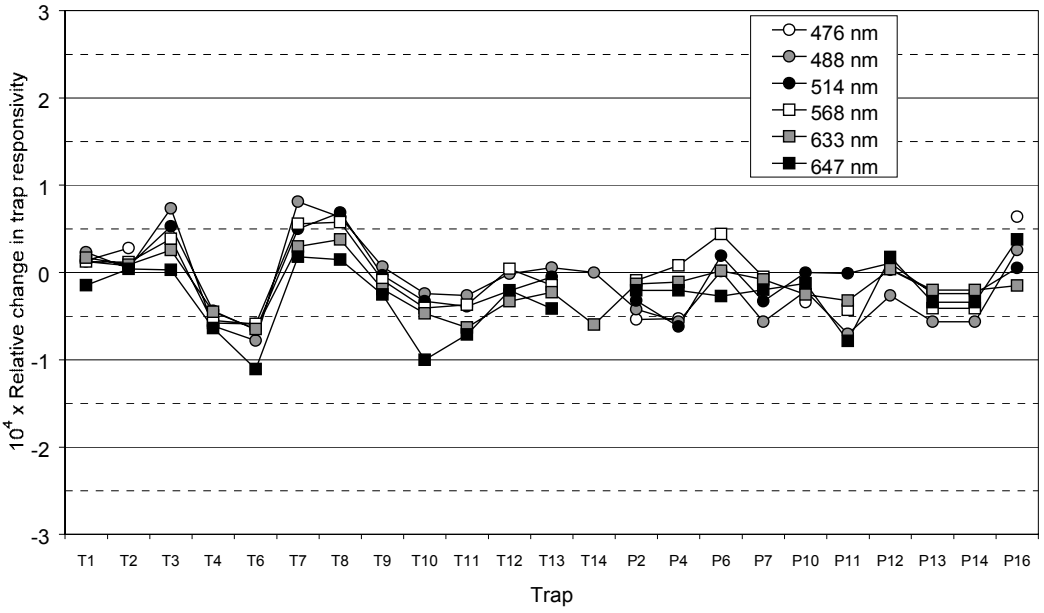

Figure 16 - Round 2. Stability of the transfer detectors compared with the reference group: relative change in responsivity at each wavelength, as measured after return to the BIPM.

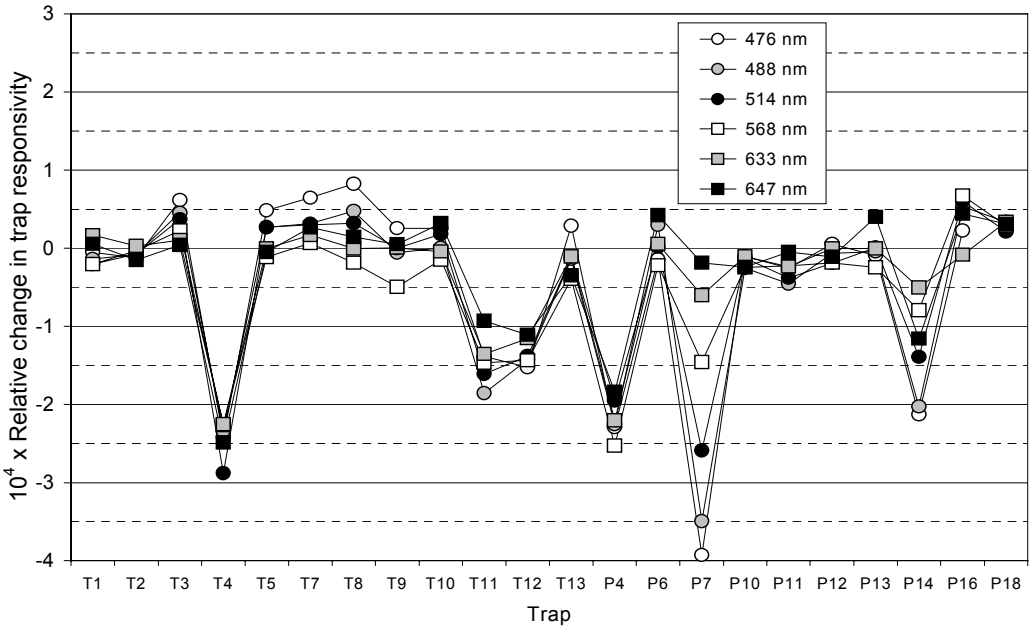

Figure 17 - Round 3. Stability of the transfer detectors compared with the reference group: relative change in responsivity at each wavelength, as measured after return to the BIPM.

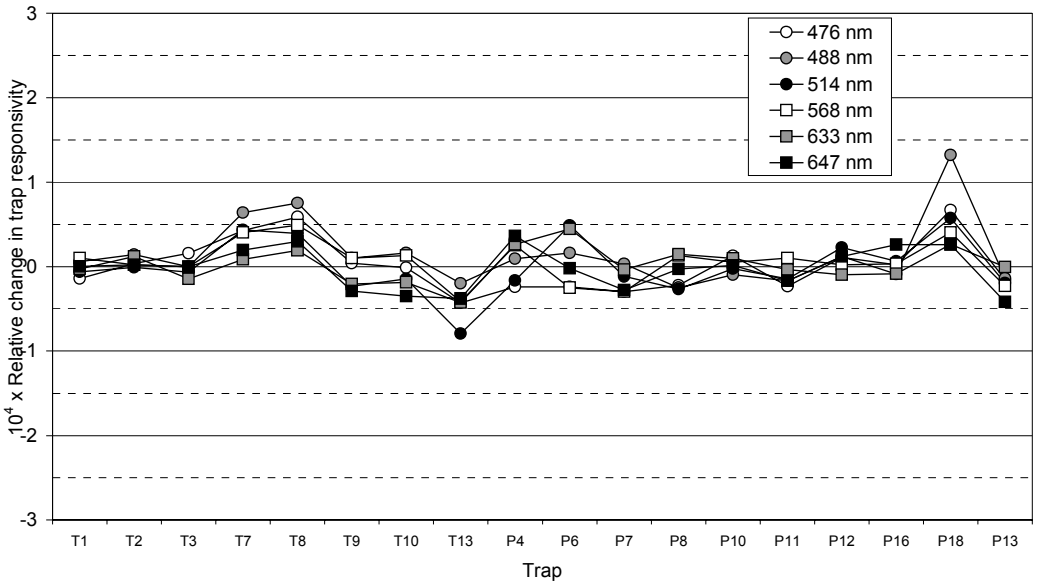

Figure 18 - Round 4. Stability of the transfer detectors compared with the reference group: relative change in responsivity at each wavelength, as measured after return to the BIPM

e) Calibrations of the reference group against the BIPM cryogenic radiometer:

For the first two rounds, the overall stability was confirmed by the repeatability of the absolute calibrations. The relative changes ranged from + 0.3×10^{-4} to -1×10^{-4}. The dispersion of the changes is consistent with the estimation of the repeatability of the absolute measurements (about 0.7×10^{-4}) with no visible wavelength dependency (see Figure 19). The reference group was therefore assumed to be stable.

After the third round (i.e. two years after the beginning of the comparison), larger changes were observed, especially at short wavelengths. But, as they were within the expanded uncertainties with a coverage factor $k = 2$, it was decided not to apply more corrections and to wait and see if the drift could be confirmed after the fourth round.

Indeed, the calibrations done after the fourth round confirmed a significant decrease of the responsivity at short wavelengths. Moreover, a careful recalculation showed that the decrease at 476 nm had been partly underestimated after the third round.

As a consequence, the results of the fourth round take into account the latest absolute calibrations, and a correction factor has been applied to the results of the third round. This additional correction factor applied to the results of the third round is shown in Table 5.

Wavelength / nm					
476	488	514	568	633	647
Correction for long-term changes					
1.00023	1.00017	1.00009	1.00011	1.00005	1.00001

Table 5 - Correction factor for long-term changes, applied to the results of the third round.

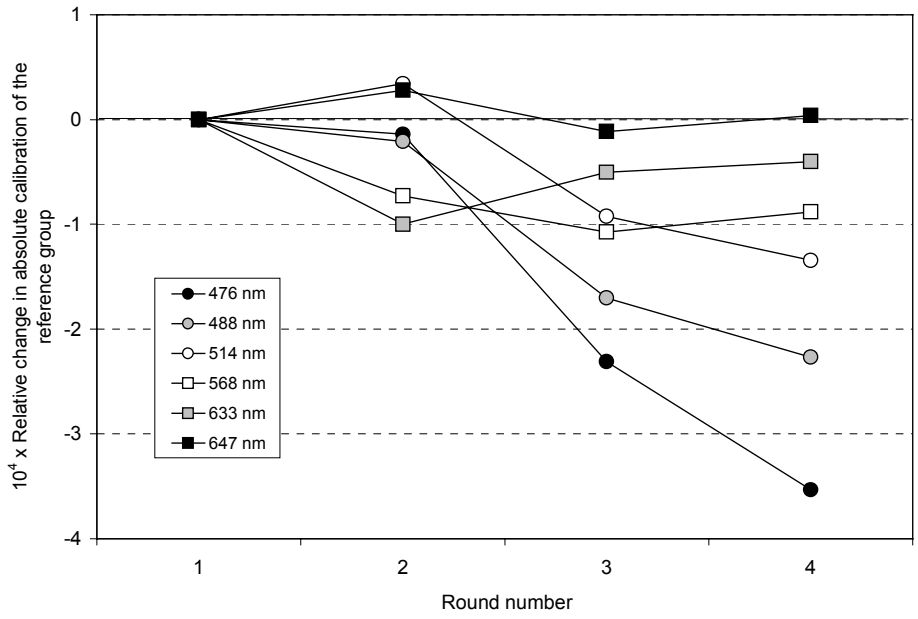

Figure 19 - Relative change in responsivity of the reference group of trap detectors, as measured by the BIPM cryogenic radiometer over the three years of the comparison.

3.2.2. Uncertainty associated with the comparison

When comparing calibrations from different laboratories, the uncertainty stated by the laboratory has to be combined with the uncertainty associated with parameters that can contribute to the variability of the results: long term-stability of the transfer detectors, temperature corrections (if used), non-linearity, non-uniformity, polarization effects.

The major contribution is that from the long-term stability of the transfer detectors. During the first two rounds, we have relied on the stability of the detectors. Experimental results show that the only reliable common reference over more than three years is the cryogenic radiometer itself. The uncertainty associated with the BIPM absolute calibrations (used to check the common reference) have therefore to be included when comparing results over the whole period.

The possible contributions are summarized in Table 6, their total being 1×10^{-4}.

Source of uncertainty	$10^4 \times$ relative standard uncertainty
Long-term stability of the transfer detectors	0.9
Temperature correction	0.2
Polarization effects	0.1
Non-linearity	0.3
Non-uniformity	0.2

Table 6 - Uncertainties associated with the transfer detectors when comparing results from different laboratories.

4. Results from the national laboratories

4.1. CSIRO

4.1.1. Experimental conditions

- Cryogenic radiometer type: Radiox, from Oxford Instruments Ltd.
- Sources: Ar/Kr mixed gas laser, Ar laser, He-Ne laser.
- Nominal power: 300 µW to 400 µW
- Beam diameter: 2 mm to 4 mm
- Temperature: 23 °C ± 1 °C

4.1.2. CSIRO uncertainty budget

In the CSIRO report, uncertainties have been reported for a 95% confidence level (at the 2 σ level). In order to keep a common presentation throughout the present document, we have calculated the corresponding standard uncertainties by dividing these values by 2, assuming a sufficiently large number of degrees of freedom (see Table 7).

Source of uncertainty	$10^4 \times$ standard uncertainty
Brewster window transmission	0.25
Cavity absorption	0.05
Repeatability	0.5
Non-equivalence	< 0.25
Electrical power	0.05
Scatter and diffraction	0.05
Total	**0.6**

Table 7 - CSIRO. Relative standard uncertainty in absolute power measurement with the cryogenic radiometer.

Source of uncertainty	$10^4 \times$ standard uncertainty
Trap alignment	0.5
Amplifier resistance	0.25
Detector size	<0.5
Total	**0.75**

Table 8 - CSIRO. Relative standard uncertainty in trap detector optical power measurements for traps P14, T11 and T12.

The relative combined expanded uncertainty (2 σ level) quoted by the CSIRO is 1.9×10^{-4}.

4.1.3. Correction factors

a) Temperature

The calibration temperatures at the BIPM and at the CSIRO differ by 2.5 °C. The following correction factors (applied to the CSIRO results) have been calculated using the temperature coefficients shown in Table 3.

	Wavelength / nm					
	476	488	514	568	633	647
Trap	Temperature correction factor					
T11	1.000038	1.000036	1.000032	1.000024	1.000015	1.000013
T12	1.000038	1.000036	1.000032	1.000024	1.000015	1.000013
P14	1.000065	1.000062	1.000056	1.000042	1.000010	1.000023

Table 9 - Correction factors used to correct the CSIRO results for the 2.5 °C temperature difference between the BIPM and the CSIRO.

b) Other factors
No other correction has been applied to the CSIRO results.

4.1.4. CSIRO: comparison with the BIPM calibrations

After temperature correction, the relative difference Δ in the calibrations is calculated for each trap, according to expression (1) in paragraph 1.3: see Table 10.

	Wavelength / nm					
	476	488	514	568	633	647
Trap	$10^4 \times$ relative difference in trap calibration					
T11	1.2	2.3	1.6	1.6	1.7	1.4
T12	0.9	2.4	2.5	2.2	1.5	1.6
P14	0.1	2.2	2.0	2.5	1.1	1.0
average	0.7	2.3	2.0	2.1	1.4	1.3

Table 10 - Relative difference in trap calibration (R_{CSIRO} - R_{BIPM}) / R_{BIPM} .

The combined relative standard uncertainty of the comparison u_C is calculated as:

$$U_C^2 = u_{CSIRO}^2 + u_{TRANSFER}^2$$

where
u_{CSIRO} is the CSIRO (2σ) relative uncertainty divided by 2: 0.95 part in 10^4
$u_{TRANSFER}$ the uncertainty associated with the transfer (see Table 6) : 1 part in 10^4
The calculated relative standard uncertainty is $u_C = 1.4 \times 10^{-4}$

4.2. HUT

4.2.1. Experimental conditions

- Cryogenic radiometer type: HUT construction
- Sources: Argon-Ion and He-Ne lasers
- Nominal power: 106 µW to 174 µW
- Beam ($1/e^2$) diameter: 2.5 mm with Argon-Ion laser and 3.5 mm with He-Ne laser approximately
- Temperature: 24 °C ± 1 °C and relative humidity of air 35% ± 5%

4.2.2. HUT uncertainty budget

The HUT uncertainty budget is given in Table 11.

Source of uncertainty	$10^4 \times$ standard uncertainty
Repeatability of the results	1.0
Window transmittance	1.0
Distance effect	1.2
Uncertainty of the DVMs	0.4
Cavity absorptance	1.0
Spatial response of trap	1.2
Relative combined standard uncertainty for calibration	**2.5**

Table 11 - HUT. Relative combined standard uncertainty for trap calibrations

4.2.3. Correction factors

a) Temperature

The calibration temperatures at the BIPM and at the HUT differ by 3.5 °C.
The following correction factors have been calculated using the temperature coefficients shown in Table 3.

	Wavelength / nm		
	488	514	633
Trap	Temperature correction factor		
P4	1.000087	1.000078	1.000036
T5	1.000050	1.000045	1.000020
T6	1.000050	1.000045	1.000020

Table 12 - Correction factors used to correct the HUT results for the 3.5 °C temperature difference between the BIPM and the HUT.

b) Other factors:

No other correction has been applied to the HUT results.

4.2.4. HUT: comparison with the BIPM calibrations

After temperature correction, the relative difference in the calibrations Δ is calculated for each trap, according to expression (1) in paragraph 1.3 :see Table 13.

	Wavelength / nm					
	476	488	514	568	633	647
Trap	$10^4 \times$ relative difference in trap calibration					
P4		2.2	0.9		-2.2	
T5		2.0	2.2		0.5	
T6		2.6	2.1		0.4	
average		2.3	1.7		-0.4	

Table 13 - Relative difference in trap calibration (R_{HUT} - R_{BIPM}) / R_{BIPM}.

The combined relative standard uncertainty of the comparison u_C is calculated as:

$u_C^2 = u_{HUT}^2 + u_{TRANSFER}^2$, where:

u_{HUT} is the HUT standard uncertainty: 2.5 parts in 10^4

$u_{TRANSFER}$ the uncertainty associated with the transfer (see Table 6) : 1 part in 10^4

The calculated relative standard uncertainty is $u_c = 2.7 \times 10^{-4}$.

4.3. SP

4.3.1. Experimental conditions

- Cryogenic radiometer type: LaseRad from Cambridge Research Institute
- Sources: He-Ne laser and Argon-Ion laser
- Nominal power: not communicated
- Beam diameter: about 2 mm
- Temperature: 23 °C to 24 °C (recorded for each trap at each wavelength).

4.3.2. SP uncertainty budget

The relative combined expanded uncertainty associated with the cryogenic radiometer is 2×10^{-4} for a coverage factor $k = 2$. However, when repeating the five series of measurements at the SP, large unexplained differences were found (up to ± 0.1%). As the source of these instabilities was not found in the course of trap calibrations, the SP estimated the associated relative uncertainty to be 1×10^{-3}.

The SP laboratory concludes that further analysis of its measurement set-up is necessary.

4.3.3. Correction factors

a) Temperature

The following correction factors were calculated using the temperature coefficients shown in Table 3.

	Wavelength / nm			
	476	488	514	633
Trap	Temperature correction factor			
T13	1.000050	1.000046	1.000041	1.000016
T14	1.000051	1.000039	1.000046	1.000016
P11	1.000094	1.000074	1.000071	1.000025

Table 14 - Correction factors used to correct the SP results for the temperature differences between BIPM and SP.

b) Wavelength

Near 476 nm, the SP used the argon laser line (vacuum wavelength 476.619 nm) whereas the BIPM and the other laboratories used the krypton line (vacuum wavelength 476.373 nm). As the difference is very small (about 0.25 nm), a linear extrapolation of the trap sensitivity was used, based on the calibration results at 476 nm and 488 nm. The SP results at 476.619 nm were therefore multiplied by the factor $C_\lambda = 0.99946$.

4.3.4. SP: comparison with the BIPM calibrations

After temperature and wavelength corrections, the relative difference in the calibrations Δ is calculated for each trap, according to expression (1) in paragraph 1.3, see Table 15.

The combined relative standard uncertainty of the comparison u_c is calculated as:

$u_C^2 = u_{SP}^2 + u_{TRANSFER}^2$, where:

u_{SP} is the SP expanded relative uncertainty ($k = 2$) divided by 2: 5 parts in 10^4

$u_{TRANSFER}$ is the uncertainty associated with the transfer (see Table 6) : 1 part in 10^4

The calculated relative standard uncertainty is $u_C = 5.1 \times 10^{-4}$

	Wavelength / nm					
	476	488	514	568	633	647
Trap	$10^4 \times$ relative difference in trap calibration					
T13	0.0	-4.9	-5.4		0.1	
T14	-4.0	-1.9	-1.7		-4.9	
P11	1.7	2.7	4.1		1.1	
average	-0.8	-1.4	-1.0		-1.3	

Table 15 - Relative difference in trap calibration (R_{SP} - R_{BIPM}) / R_{BIPM} .

In spite of a large dispersion of the individual results, the average values are very close to the results obtained by the other laboratories.

4.4. NIST

4.4.1. Experimental conditions

- Cryogenic radiometer type: vertical system, developed by the NIST on the basis of an Oxford Instruments-NPL design.
- Source: He-Ne laser and Ar laser.
- Nominal power:
  0.28 mW with the Ar laser, and 0.58 mW with the He-Ne laser
- Beam diameter: 2 mm with Ar laser and 1.7 mm with He-Ne laser
- Temperature: stated for each wavelength (21.2 °C to 22.8 °C)

4.4.2. NIST uncertainty budget

Source of uncertainty Type B	$10^4 \times$ relative standard uncertainty	
	wavelength	
	514 nm and 488 nm	633 nm
Window transmittance	0.9	2.6
Scattered optical power	1.3	1.3
Cavity absorptance	0.2	0.2
Temperature gradients	0.4	0.4
Heater power	0.3	0.3
Standard resistor	0.03	0.03
Amplifier gain	1.0	1.0
Voltage measurements	0.3	0.3
Combined	**2.0**	**2.6**

Table 16 - NIST uncertainty budget.

Trap	$10^4 \times$ combined uncertainty		
	Wavelength		
	633 nm	488 nm	514 nm
T3	3.4	4.4	3.1
T13	3.4	4.4	3.0
P11	5.3	4.4	3.0

Table 17 - NIST. Relative combined (type A and type B) standard uncertainty in trap detector calibration.

4.4.3. Correction factors

a) Temperature:

The following temperature correction factors have been calculated using the temperature coefficients shown in Table 3.

	Temperature correction factor		
	wavelength		
Trap	488	514	633
T3	1.000030	1.000027	1.000010
T13	1.000030	1.000027	1.000010
P11	1.000052	1.000047	1.000018

Table 18 - Correction factors used to correct the NIST results for the temperature difference between the BIPM and the NIST

b) Non-linearity:

At 633 nm the beam diameter used was 1.7 mm with an optical power of 0.58 mW. These parameters correspond to the beginning of the non-linear region of the transfer detectors (see section 2.1.4). After their return to the BIPM, a specific measurement of their non-linearity was made, using exactly these parameters.
The measured non-linearity was -0.3×10^{-4}, and the NIST calibrations results have been corrected for this effect. The effects of non-linearity on the transmission trap and on the reflection trap are very similar. This cannot explain the lack of consistency (about 6 parts in 10^4, see Table 19) of the results obtained from both types at this wavelength.

4.4.4. NIST: comparison with the BIPM calibrations

The results given here are different from those shown in the Progress Report (Part I), transmitted to the participating laboratories in June 1997. At that time, as technical problems were experienced with its argon laser, the NIST calibrated the transfer detectors only at the He-Ne red line. The average relative difference between the BIPM calibration and the calibration reported by the NIST in March 1997 was found to be:

$(+3.0 \times 10^{-4})$ at 633 nm. (see Figure 22)

The NIST decided to participate in the fourth round and was asked to calibrate three other traps. The results presented here are part of this fourth round (September 1998 to February 1999).

After corrections, including long-term drifts, the relative difference of the calibration Δ is calculated for each trap, according to expression (1) in paragraph, see Table 19.

	Wavelength / nm					
	476	488	514	568	633	647
Trap	$10^4 \times$ relative difference in trap calibration					
T3		7.0	6.1		4.8	
T13		7.9	6.1		5.2	
P11		7.1	5.9		–1.4	
average		7.3	5.9		2.9	

Table 19 - Relative difference in trap calibration $(R_{NIST} - R_{BIPM}) / R_{BIPM}$.

The results at $\lambda = 633$ nm confirm the order of magnitude of the difference between the NIST and the BIPM seen during the first round.

The combined relative standard uncertainty of the comparison u_C is calculated as:
$u_C^2 = u_{NIST}^2 + u_{TRANSFER}^2$, where
u_{NIST} is the NIST relative uncertainty given for each detector
$u_{TRANSFER}$ is the uncertainty associated with the transfer (see Table 6) : 1 part in 10^4
The relative combined standard uncertainty is given in Table 20.

	$10^4 \times$ combined uncertainty		
	wavelength		
Trap	488	514	633
T3	4.5	3.2	3.5
T13	4.5	3.2	3.5
P11	4.5	3.3	5.4

Table 20 - NIST. Relative combined standard uncertainty of the comparison.

4.5. NPL

4.5.1. Experimental conditions

Cryogenic radiometer type: Mechanically cooled Cryogenic Radiometer, from Oxford Instruments Ltd.
Source: Ar laser and Kr laser
Nominal power: 400 μW to 500 μW
Beam diameter: 3 mm to 4 mm
Temperature: not specified

4.5.2. NPL uncertainty budget

The NPL relative standard uncertainties associated with the trap calibrations are shown in Table 21.

	Wavelength / nm					
	476	488	514	568	633	647
Trap	$10^4 \times$ standard uncertainty of trap calibration					
T9	0.5		0.4	0.4		0.7
T10	0.5		0.4	0.3		0.6
P7	0.6		0.3	0.4		0.4

Table 21 - NPL relative standard uncertainties associated with the trap calibrations.

For more details see also [5, 4, 3].

4.5.3. Correction factors

No correction was applied to the NPL results.

4.5.4. NPL: comparison with the BIPM calibrations

The relative difference of the calibration Δ calculated for each trap according to expression (1) in paragraph 1.3 , is shown in Table 22.

	Wavelength / nm					
	476	488	514	568	633	647
Trap	Relative difference in trap calibration / 10^{-4}					
T9	0.1		2.1	2.2		2.0
T10	-0.4		1.5	1.5		1.3
P7	-0.6		0.5	1.9		0.9
average	-0.3		1.3	1.9		1.4

Table 22 - Relative difference in trap calibration ($R_{NPL} - R_{BIPM}$) / R_{BIPM} .

The combined relative standard uncertainty of the comparison u_c is calculated as:
$u_c^2 = u_{NPL}^2 + u_{TRANSFER}^2$
where u_{NPL} is the NPL relative uncertainty given for each detector.
$u_{TRANSFER}$ is the uncertainty associated with the transfer,
with no temperature correction (see Table 6) : 1 part in 10^4

The calculated relative standard uncertainty is given in Table 23.

	Wavelength / nm			
	476	514	568	647
Trap	$10^4 \times$ standard uncertainty of the comparison			
T9	1.1	1.1	1.0	1.2
T10	1.1	1.1	1.1	1.2
P7	1.2	1.0	1.1	1.1

Table 23 - Relative combined standard uncertainty of the comparison (NPL).

4.6. BNM-INM

4.6.1. Experimental conditions

- Cryogenic radiometer type: LaseRad from the Cambridge Research Institute
- Sources: He-Ne laser and argon laser
- Nominal power: 150 μW
- Beam diameter ($1/e^2$): 1 mm
- Temperature: about 24 °C

4.6.2. BNM-INM uncertainty budget

In this study, the BNM divided the Type B uncertainties into three groups: those related to the measurement of the transfer detector photocurrent, those related to the experimental arrangement and those related to the cryogenic radiometer itself. In the first group, the major contribution to the uncertainty is from the calibration of the current-voltage converter used to measure the photocurrent. In the second group, the major contribution is associated with the corrections due to the difference in diameter between the detectors and the cavity of the radiometer (referred to as the diaphragm effect). In the third group, the uncertainty associated with the cryogenic radiometer takes into account the cavity absorptance [21], the window transmittance, the non-equivalence of electrical heating and optical heating, and the electrical calibration of the system.

Source of uncertainty	$10^4 \times u_B$
Current/voltage converter calibration	0.5
Diaphragm effect	0.1 to 0.2
Cryogenic radiometer	0.5
Total	0.74

Table 24 - BNM-INM: Type B uncertainties u_B of the calibration.

The Type A uncertainties were calculated for each detector from the relative standard deviation of the series of measurements over the whole period of calibration.

Transfer detector	Wavelength / nm		
	488	514	633
	$10^4 \times u_A$		
T4	1.3	1.0	0.7
T6	1.3	1.1	0.5
P4	2.0	1.4	0.7

Table 25 - BNM-INM: Type A uncertainties u_A of the calibration.

Transfer detector	Wavelength / nm		
	488	514	633
	$10^4 \times u_C$		
T4	1.5	1.2	1.0
T6	1.5	1.3	0.9
P4	2.1	1.6	1.0

Table 26 – BNM-INM: Relative combined standard uncertainty u_C for the calibration of the transfer detectors.

4.6.3. Correction factors

a) Temperature

The calibration temperatures at the BIPM and at the BNM-INM differ by 3.5 °C. The following correction factors have been calculated using the temperature coefficients given in section 2.1.2.

Transfer detector	Wavelength / nm		
	488	514	633
	Temperature correction factor		
P4	1.000087	1.000078	1.000036
T4	1.000050	1.000045	1.000020
T6	1.000050	1.000045	1.000020

Table 27 - Correction factors used to correct the BNM-INM results for the 3.5 °C temperature difference between the BIPM and the BNM-INM.

b) Linearity

With the relatively small laser beam diameter used (1 mm), the BNM reduced the optical power of the calibration to 150 μW, as recommended in the documents sent together with the transfer detectors, in order to avoid non-linearity effects (see section 2.1.4). Therefore, no correction has been applied to the BNM results.

4.6.4. Comparison with the BIPM calibrations

The results given here are different from those shown in the Progress Report (Part II), transmitted to the participating laboratories in April 1998. The average relative differences between the BIPM calibrations and the calibrations reported by the BNM-INM in January 1998 were found to be:

(-0.8×10^{-4}) at 488 nm,
(-1.3×10^{-4}) at 514 nm
(-1.8×10^{-4}) at 633 nm. (see Figure 22)

The BIPM Progress Report showed that the calibrations were in agreement within the uncertainties of the comparison, but significantly different from those obtained in a previous direct BNM / BIPM comparison in 1994 (see section 5.3). At that time, the difference was found to be + 1.9 parts in 10^4 at $\lambda = 647$ nm.
The BNM-INM therefore decided to check its data reduction of the measurements related to the transfer detectors, and found that the value of the gain of its current/voltage converter was not correct: the value used was not the latest gain calibration result but an older value.

The corrected calibration results, taking into account the real gain value, have been communicated to the BIPM in October 1998. They are shown in Table 28.

Transfer detector	Wavelength / nm					
	476	488	514	568	633	647
	$10^4 \times$ Relative difference in trap calibration					
T4		1.8	1.7		1.4	
T6		2.2	1.4		–0.8	
P4		1.2	0.2		1.2	
average		1.8	1.1		0.6	

Table 28 - Relative difference in trap calibration: $(R_{BNM} - R_{BIPM}) / R_{BIPM}$.

The combined relative standard uncertainty of the comparison u_c is calculated using:

$$u_C^2 = u_{BNM}^2 + u_{TRANSFER}^2$$

where u_{BNM} is the BNM-INM relative uncertainty given for each detector.

$u_{TRANSFER}$ is the uncertainty associated with the transfer, that is 1×10^{-4} (see Table 6).
In graphs, the uncertainty associated with the average difference is calculated as the quadratic mean of the uncertainties associated with each individual detector.

Transfer detector	Wavelength / nm		
	488	514	633
	$10^4 \times u_C$		
T4	1.8	1.6	1.4
T6	1.8	1.6	1.3
P4	2.3	1.9	1.4

Table 29 - Relative combined standard uncertainty of the comparison (BNM-INM).

4.7. PTB - Radiometry laboratory (Braunschweig)

As two different laboratories from the PTB are involved in this comparison, to avoid confusion the PTB - Radiometry laboratory (Braunschweig) will be denoted in graphs as PTB-R.

4.7.1. Experimental conditions

- Cryogenic radiometer type: LaseRad from the Cambridge Research Institute
- Sources: He-Ne laser and argon laser
- Temperature: 20.6 °C to 20.8 °C, specified for each calibration.

The transfer detectors used in the comparison are known to be non-linear if used at a high level of irradiance. For a given optical power, irradiance increases when the beam diameter decreases, making the beam diameter a critical parameter (see section 2.1.4). The PTB experimental arrangement is optimized for laser beam diameters of the order of 0.9 mm ($1/e^2$). To avoid non-linearity effects in the transfer detectors, the PTB calibration chain was organized as follows:

a) The PTB primary standard is the LaseRad II cryogenic radiometer.
b) A set of three PTB trap detectors made from Hamamatsu 1227 photodiodes (known for their good linearity) was calibrated at each of the three wavelengths selected for the comparison.
c) Each BIPM transfer detector was then calibrated by direct comparison with the PTB set, at each wavelength, using the same beam size but at a radiant power as low as 64 µW.

The parameters used during step (c) are summarized in Table 30.

Laser		Wavelength / nm	$10^4 \times$ Standard uncertainty	Beam diameter ($1/e^2$) / µm	Radiant power / µW	Temperature / °C
P6	Ar^+	488	1.9	860	65	20.7
	Ar^+	514.5	2.7	840	65	20.7
	HeNe	632.8	1.0	860	64	20.6
T7	Ar^+	488	1.9	860	65	20.7
	Ar^+	514.5	2.7	840	65	20.6
	HeNe	632.8	1.0	860	64	20.6
T8	Ar^+	488	1.9	860	65	20.8
	Ar^+	514.5	1.5	840	65	20.6
	HeNe	632.8	2.7	860	64	20.6

Table 30 – Parameters for the calibration of the transfer detectors at the PTB.

4.7.2. PTB uncertainty budget

The relative standard uncertainty of the calibration is 1×10^{-4} to 2.7×10^{-4} as shown in Table 30. For more details, see also [22, 23, 24].

4.7.3. Correction factors

The results were corrected for the small temperature difference between the BIPM and the PTB (0.1 °C to 0.3 °C). This correction is almost negligible (a few parts in 10^6).

4.7.4. Comparison with the BIPM calibrations

The results given here are different from those shown in the BIPM Progress

Report (Part II), transmitted to the participating laboratories in April 1998. The average relative differences between the BIPM calibrations and the calibrations reported by the PTB in February 1998 were found to be:

(8.1×10^{-4}) at 488 nm,
(5.7×10^{-4}) at 514 nm
(2.5×10^{-4}) at 633 nm. (see Figure 22)

The difference found at λ = 633 nm was practically the same as that found in 1995 by direct comparison at the PTB [24], that is 2.3×10^{-4}. However, the BIPM report pointed out that further investigation was probably necessary to explain the increase of the deviation at 514 nm and 488 nm.
Indeed, the PTB sent a revised final version of the calibrations in December 1998, which explains that in the previous version the window transmittance as measured at 633 nm was also used for the other wavelengths. After completion of the window transmittance measurements at 488 nm and 514 nm, the corresponding detector calibrations and uncertainties have been revised. The relative difference in the calibrations, based on this final report, is shown in Table 31.

Transfer detector	Wavelength / nm					
	476	488	514	568	633	647
	$10^4 \times$ Relative difference in trap calibration					
T7		2.9	3.2		2.3	
T8		3.3	3.0		2.3	
P6		3.5	2.5		2.8	
average		3.2	2.9		2.5	

Table 31 - Relative difference in trap calibration: $(R_{\text{PTB-R}} - R_{\text{BIPM}}) / R_{\text{BIPM}}$.

The combined relative standard uncertainty of the comparison u_C is calculated using:

$$u_C{}^2 = u_{\text{PTB}}{}^2 + u_{\text{TRANSFER}}{}^2$$

where u_{PTB} is the PTB relative uncertainty given for each detector.
u_{TRANSFER} is the uncertainty associated with the transfer, that is 1×10^{-4}

Transfer detector	Wavelength / nm		
	488	514	633
	$10^4 \times u_C$		
T7	2.1	2.9	1.4
T8	2.1	2.9	1.4
P6	2.1	2.9	1.4

Table 32 - Relative combined standard uncertainty of the comparison (PTB-R).

4.8. IFA

4.8.1. Experimental conditions

- Cryogenic radiometer type: LaseRad from the Cambridge Research Institute
- Sources: He-Ne laser, Kr laser and Ar laser
- Nominal power: 400 µW
- Beam diameter ($1/e^2$): 2 mm
- Temperature: about 20.5 °C ± 1 °C.

4.8.2. IFA uncertainty budget

Source of uncertainty	$10^4 \times$ Standard uncertainty
Photocurrent meter resolution	0.58
Photocurrent measurement noise	0.50
Pico-ammeter calibration factor	0.042
Cryogenic radiometer accuracy	1.3
Cryogenic radiometer linearity	1.0
Cryogenic radiometer measurement noise	0.6
Window throughput	0.45

Table 33 - IFA uncertainty budget for the calibration of the transfer detectors.

The estimated relative combined standard uncertainty of the calibration is 2×10^{-4} (4×10^{-4} for a coverage factor $k = 2$).

4.8.3. Correction factors

No correction was applied to the IFA results.

4.8.4. Comparison with the BIPM calibrations

Transfer detector	Wavelength / nm					
	476	488	514	568	633	647
	$10^4 \times$ Relative difference in trap calibration					
T9	4.5		1.9	0.8	–3.4	3.3
T10	2.1		–2.9	–2.4	–5.7	0.5
P7	3.4		1.2	0.0	–4.7	2.2
average	3.4		0.0	–0.5	–4.6	2.0

Table 34 - Relative difference in trap calibration: $(R_{IFA} - R_{BIPM}) / R_{BIPM}$.

The combined relative standard uncertainty of the comparison u_C is calculated using:

$$u_C^2 = u_{IFA}^2 + u_{TRANSFER}^2$$

where u_{IFA} is the IFA relative uncertainty: 2×10^{-4}.

$u_{TRANSFER}$ is the uncertainty associated with the transfer: 1×10^{-4} (see Table 6).

Therefore $u_C = 2.2 \times 10^{-4}$.

The dispersion of the results is rather large, up to 8×10^{-4} between 633 nm and 476 nm, but it is consistent with the stated uncertainties.

4.9. MSL

4.9.1. Experimental conditions

- Cryogenic radiometer type: Radiox, from Oxford Instruments Ltd.
- Sources: He-Ne laser and argon laser
- Nominal power: 50 µW to 150 µW
- Temperature: 20 °C

Wavelength / nm	$1/e^2$ beam diameter / mm	Radiant intensity / μW
488	2.2	123 to 143
514	2.2	126 to 200
633	1.5	52

Table 35 - Beam diameter and optical power used by the MSL.

4.9.2. MSL uncertainty budget

The MSL uncertainty budget is given in Table 36. A detailed study of calibration procedures at the MSL and uncertainty calculations was also published elsewhere [25].

Source of uncertainty	Wavelength / nm								
	488			514			633		
	$10^4 \times$ standard uncertainty								
Radiox power measurement	0.29			0.50			0.96		
Window transmittance	0.26			0.54			0.1		
Cavity absorptance	0.05			0.05			0.05		
Heating non-equivalence	0.1			0.1			0.1		
Standard resistor	0.06			0.06			0.06		
Digital voltmeter	0.1			0.1			0.1		
Current/voltage converter	0.14			0.14			0.14		
Transfer detector:	P14	T12	T11	P14	T12	T11	P14	T12	T11
Beam geometry	0.25	0.20	0.20	0.25	0.20	0.20	0.28	0.20	0.20
Trap signal	0.21	0.12	0.10	0.12	0.16	0.11	0.08	0.07	0.10
Quadrature sum of above	0.6	0.5	0.5	0.8	0.8	0.8	1.0	1.0	1.0

Table 36 - MSL: uncertainty budget for the calibration of the transfer detectors.

4.9.3. Correction factors

The results were corrected for the small temperature difference between the BIPM and the MSL (0.5 °C).

Transfer detector	Wavelength / nm		
	488	514	633
	Temperature correction factor		
T11	0.999993	0.999994	0.999997
T12	0.999993	0.999994	0.999997
P14	0.999988	0.999989	0.999997

Table 37 - Correction factors used to correct the MSL results for the 0.5 °C temperature difference between the BIPM and the MSL.

4.9.4. Comparison with the BIPM calibrations

The results given here are slightly different from those shown in the BIPM Progress Report (Part II), transmitted to the participating laboratories in April 1998. The average relative differences between the BIPM calibrations and the preliminary calibration values reported by the MSL were found to be:

(0.6×10^{-4}) at 488 nm, (0.9×10^{-4}) at 514 nm , (0.0×10^{-4}) at 633 nm.

(see Figure 22)

After checking its data analysis, the MSL sent revised values in a final calibration report. The relative differences between the BIPM calibrations and the MSL calibrations are shown in Table 38.

Transfer detector	Wavelength / nm					
	476	488	514	568	633	647
	$10^4 \times$ Relative difference in trap calibration					
T11		0.9	1.2		1.1	
T12		0.5	0.0		0.9	
P14		–0.1	–0.2		–0.2	
average		0.4	0.3		0.6	

Table 38 - Relative difference in trap calibration: $(R_{MSL} - R_{BIPM}) / R_{BIPM}$.

The combined relative standard uncertainty of the comparison u_C is calculated using:

$$u_C^2 = u_{MSL}^2 + u_{TRANSFER}^2$$

where u_{MSL} is the MSL relative uncertainty given for each detector.

$u_{TRANSFER}$ is the uncertainty associated with the transfer, that is 1×10^{-4} .

Transfer detector	Wavelength / nm		
	488	514	633
	$10^4 \times$ Standard uncertainty		
T11	1.1	1.3	1.4
T12	1.1	1.3	1.4
P14	1.2	1.3	1.4

Table 39 - Relative combined standard uncertainty of the comparison (MSL).

4.10. DFM

The results given here are different from those shown in the BIPM Progress Report (Part II), transmitted to the participating laboratories in April 1998.

The average relative differences between the BIPM calibrations and the calibrations reported by the DFM in February 1998 were found to be:

$(+23.6 \times 10^{-4})$ at 476 nm
$(+22.1 \times 10^{-4})$ at 488 nm
$(+ 9.2 \times 10^{-4})$ at 514 nm
$(+20.7 \times 10^{-4})$ at 568 nm
$(+11.9 \times 10^{-4})$ at 633 nm
$(+14.6 \times 10^{-4})$ at 647 nm (see Figure 22)

The differences in calibration obtained were much larger than one would reasonably expect in such a comparison. The DFM decided to check and modify its experimental arrangement and participated in the fourth round of the comparison.
The results presented here for a new batch of transfer detectors are part of this fourth round (September 1998 to February 1999).

4.10.1. Experimental conditions

- Cryogenic radiometer type: Radiox, from Oxford Instruments Ltd.
- Sources: He-Ne laser, Ar / Kr mixed gas laser
- Nominal power: 200 μW to 400 μW
- Beam diameter: 2 mm to 3 mm

- Temperature: 23 °C

The DFM reports that several changes have been made to its experimental arrangement since the previous round. They are all related to the preparation of the optical beam: modification of the intensity stabilization system, installation of an additional polarizer. This allowed a much better control of the shape and of the polarization state of the beam.

4.10.2. DFM uncertainty budget

The estimated relative combined standard uncertainty is 2.3×10^{-4}.
(No detailed budget).

4.10.3. Correction factor

Transfer detector	Wavelength / nm					
	476	488	514	568	633	647
	Temperature correction factor					
T9	1.000038	1.000036	1.000032	1.000024	1.000015	1.000013
T10	1.000038	1.000036	1.000032	1.000024	1.000015	1.000013
P18	1.000065	1.000062	1.000056	1.000042	1.000026	1.000023

Table 40 - Correction factors used to correct the DFM results for the 2.5 °C temperature difference between the BIPM and the DFM.

4.10.4. Comparison with the BIPM calibrations

After corrections, including long-term drifts, the relative difference in the calibrations Δ is calculated for each trap, as shown in Table 41.

Transfer detector	Wavelength / nm					
	476	488	514	568	633	647
	$10^4 \times$ Relative difference in trap calibration					
T9	-2.5	-0.4	0.2	-2.4	-1.2	-1.1
T10	-1.0	0.6	-0.7	-2.5	-0.6	0.2
P18	-2.4	3.0	-0.4	-0.1	-0.8	0.4
average	-2.0	1.1	-0.3	-1.7	-0.8	-0.2

Table 41 - Relative difference in trap calibration: $(R_{DFM} - R_{BIPM}) / R_{BIPM}$.

The combined relative standard uncertainty of the comparison u_C is calculated using:

$u_C^2 = u_{DFM}^2 + u_{TRANSFER}^2$

where u_{DFM} is the DFM relative uncertainty: 2.3×10^{-4}.

$u_{TRANSFER}$ is the uncertainty associated with the transfer, that is 1×10^{-4}

Therefore $u_C = 2.5 \times 10^{-4}$.

This much better agreement confirms again that the quality of the beam preparation is crucial in high-accuracy cryogenic radiometry.

4.11. NRC

The NRC has developed a monochromator-based spectral calibration facility for transfer standard radiometers, using a cryogenic radiometer. This choice [26, 27] was made for practical reasons: although the accuracy is not as good as that of laser-based systems, the spectral coverage is much better, the measurement can be fully automated, and overall costs are greatly reduced.

The detector to be calibrated and the cryogenic radiometer are placed in a

windowed hermetically sealed enclosure. As the calibration is done under vacuum, it is not possible to calibrate the BIPM transfer detectors directly against the cryogenic radiometer. Instead, they were calibrated in two steps using six NRC transfer radiometers, which were themselves calibrated using the cryogenic radiometer facility.

4.11.1. Experimental conditions

Calibration of NRC transfer radiometers:

- Cryogenic radiometer type: Cambridge Research and Instrumentation, optimized for monochromator-based sources.
- Source: single monochromator in conjunction with a tungsten-halogen lamp, *f*/8 beam.

Calibration of the BIPM traps using the NRC transfer radiometers:

- Source: single monochromator, bandpass of 5 nm FWHM, *f*/14 beam, focused inside the trap, 1 cm beyond the aperture.
- Spot size: rectangular-shaped at the focus, 1.5 mm by 3.0 mm approximately. Limiting apertures of 6.0 mm diameter were used with the BIPM traps, a size which matches the diameter of the apertures used on the NRC transfer radiometers.
- Nominal power: 1μW to 3 μW in all cases.
- Polarization: the degree of polarization varies from a maximum of about 12% at 476 nm to a minimum of 2% at 568 nm; the principal polarization direction is vertical with the traps oriented as shown in the BIPM measurement protocol.
- Temperature: 23.2 °C to 23.3 °C

4.11.2. NRC uncertainty budget

Source of uncertainty	$10^4 \times$ Standard uncertainty	
	Type A	Type B
Cryorad cavity absorptance		1
Cryorad electrical power measurement		1
Cryorad non-equivalence effects		1
Transfer radiometer photocurrent measurement		1
Wavelength errors		1.5
Bandwidth effects		1
Repeatability	2.5	
Combined uncertainty	2.5	2.7

Table 42 - Uncertainty budget for the calibration of NRC radiometers using the cryogenic radiometer facility.

Source of uncertainty	$10^4 \times$ Standard uncertainty	
	Type A	Type B
Repeatability: noise, alignment, etc.	1	
Geometrical and electrical effects: amplifier signal, alignment technique, vignetting, polarization, wavelength errors, stray light, bandwidth errors, etc.		1.5

Table 43 - Uncertainty budget for the calibration of BIPM traps using NRC transfer radiometers and auxiliary apparatus.

	$10^4 \times$ combined standard uncertainty	
	Type A	Type B
Calibration of one BIPM trap using one NRC radiometer	2.7	3.1
Calibration of one BIPM trap using six NRC radiometers	1.1	3.1
Combined relative standard uncertainty for the calibration of one BIPM trap using six NRC radiometers	3.3	

Table 44 - Combined relative standard uncertainty for the calibration of one BIPM trap using six NRC radiometers.

4.11.3. Correction factors

a) Temperature correction:

The results were corrected for the temperature difference between the BIPM (20.5°C) and the NRC (23.2 °C to 23.3 °C), using the temperature coefficients given in section 2.1.2.

	Wavelength / nm					
	476	488	514	568	633	647
Trap	Temperature correction factor					
T7	1.000041	1.000039	1.000035	1.000026	1.000016	1.000016
T8	1.000041	1.000039	1.000035	1.000026	1.000016	1.000016
P6	1.000070	1.000067	1.000060	1.000046	1.000028	1.000024

Table 45 - Correction factors used to correct the NRC results for the temperature difference between the BIPM and the NRC.

b) Wavelength correction:

The BIPM measurement protocol states that the calibration of the transfer detectors should be done at some specific laser line wavelengths. The laser wavelengths in air to be used were given with only one decimal digit: this was perhaps somewhat misleading, because the two laboratories using monochromator-based facilities have used the rounded wavelength values shown in column 2 of Table 46.

In order to compare more accurately their results with those from laboratories using laser sources, the results were corrected for the small wavelength difference found when the wavelength is given with more decimal digits [28]. The correction factors were calculated by two means: either by simple linear extrapolation, or using a theoretical model of the trap detectors. Results were identical within a few parts in 10^6.

Laser wavelength / nm	Monochromator wavelength / nm	Correction factor
476.243	476.2	1.00009
487.986	488	0.99997
514.536	514.5	1.00007
568.188	568.2	0.99998
632.817	632.8	1.00003
647.089	647.1	0.99998

Table 46 - Wavelength correction

The corrections are very small, in any case much smaller than the uncertainties of the calibrations.

c) Polarization correction:

The trap detectors constructed at the BIPM exhibit a residual sensitivity to the polarization state of the beam (see section 2.1.3). For that reason, they have to be calibrated and used always oriented the same way with respect to the direction of polarization. The following procedure was used to determine the change in responsivity when the source is unpolarized:

- the responsivity R_0 of the detector is measured when aligned as usual, in a linearly polarized laser beam;
- it is then rotated by 90° about the beam axis, and the responsivity R_{90} is obtained;
- the average value R_{avg} of the two responsivities is a close approximation of the responsivity in an unpolarized beam. The correction factor to be applied is therefore equal to R_{avg} / R_0.

This factor has to be determined for each detector. Experimental values are given in Table 47.

	Wavelength / nm					
	476	488	514	568	633	647
Trap	Polarization correction factor					
P6	1.00004	1.00004	1.00004	1.00004	1.00004	1.00004
T7 & T8	1.000015	1.000015	1.000015	1.000015	1.000015	1.000015

Table 47 - Polarization correction factor to be applied to the responsivity values obtained with an unpolarized source instead of the linearly polarized beam.

The corrections are small but not negligible, especially for P6.

As the degree of polarization of the beam at the output of the NRC monochromator ranges from 2% to 12%, the correction corresponding to a perfectly unpolarized beam was applied. The error introduced by this approximation is negligible when compared with the other sources of uncertainty.

4.11.4. Comparison with the BIPM calibrations

After corrections, including long-term drifts (see Table 5), the relative difference in the calibrations Δ is calculated for each trap as shown in Table 48.

Transfer detector	Wavelength / nm					
	476	488	514	568	633	647
	$10^4 \times$ Relative difference in trap calibration					
T7	1.7	4.9	5.7	5.3	5.0	4.7
T8	1.6	5.0	5.5	5.7	5.1	4.6
P6	0.9	3.9	4.8	4.6	4.3	3.8
average	1.4	4.6	5.3	5.2	4.8	4.4

Table 48 - Relative difference in trap calibrations $(R_{NRC} - R_{BIPM}) / R_{BIPM}$.

The combined relative standard uncertainty of the comparison u_C is calculated using:

$$u_C^2 = u_{NRC}^2 + u_{TRANSFER}^2$$

where u_{NRC} is the NRC relative uncertainty,

$u_{TRANSFER}$ is the uncertainty associated with the transfer: 1×10^{-4} (see Table 6).

The calculation gives: $u_C = 3.4 \times 10^{-4}$.

4.12. NMi-VSL

The NMi-VSL is also a laboratory using a monochromator-based facility for the calibration of transfer detectors under vacuum. As the BIPM transfer detectors should not be calibrated under vacuum, the measurements have been performed in two steps. First, NMi transfer standards (vacuum reflection traps) have been calibrated against the cryogenic radiometer, using a monochromator in conjunction with a QTH lamp as a source. In a second step, the BIPM transfer detectors have been calibrated against the NMi standards.

The NMi detectors are designed to accept an *f*/8 optical beam at the entrance aperture. During the second step, however, the BIPM detectors showed vignetting problems using this set-up, because they had to be placed in the diverging part of the optical beam. This was checked by performing the transfer also with lasers. To reduce the vignetting effects, the monochromator optical beam was reduced to about f/20. With this reduction, the differences between the laser and monochromator calibrations decreased to below one part in 10^4.

4.12.1. Experimental conditions

Primary reference:

- Cryogenic radiometer type: Cambridge Research and Instrumentation, optimized for monochromator-based sources.
- NMI transfer detectors calibrated under vacuum.

Details on calibration procedures are given in [29].

Calibration transfer from NMi detectors to BIPM detectors:
A 6 mm diameter aperture was placed in front of the BIPM detectors. The aperture diameter matches that of the NMi transfer detectors.

- Monochromator bandwidth : 5 nm
- f-number: f/20 approximately
- Spot size 4.5 mm
- Optical power 2.5 µW to 9 µW
- Temperature: 21.5 °C ± 0.5 °C
- Relative humidity 45% ± 10%

4.12.2. NMI-VSL uncertainty budget

Source of uncertainty	10^4 × Standard uncertainty	
	Type A	Type B
Typical repeatability	0.5	
NMi transfer standards VT1 and VT3		2.0
Current measurements		0.7
Stray light and vignetting		1.0
Sum in quadrature	0.5	2.3
Combined standard uncertainty	2.4	

Table 49 - NMI-VSL uncertainty budget for the calibration of the BIPM transfer detectors.

4.12.3. Correction factors

a) Temperature correction:

The results were corrected for the temperature difference between the BIPM (20.5 °C) and the NMi-VSL (21.5 °C), using the temperature coefficients given in 2.1.2.

	Wavelength / nm					
	476	488	514	568	633	647
Trap	Temperature correction factor					
T3	1.000015	1.000014	1.000013	1.000010	1.000006	1.000005
T13	1.000015	1.000014	1.000013	1.000010	1.000006	1.000005
P11	1.000026	1.000025	1.000022	1.000017	1.000010	1.000009

Table 50 - Correction factors used to correct the NMi-VSL results for the temperature difference between the BIPM and the NMi-VSL.

b) Wavelength correction:

The same wavelength correction as for the NRC results have been applied. (see Table 46)

c) Polarization correction:

As for the NRC, the results have been corrected for the effects of the unpolarized source on the responsivity of the BIPM detectors (see 2.1.3). The experimental values are very similar to those shown in Table 47 concerning the detectors sent to the NRC.

	Wavelength / nm					
	476	488	514	568	633	647
Trap	Polarization correction factor					
P11	1.00005	1.00005	1.00005	1.00005	1.00005	1.00005
T3 & T13	1.000015	1.000015	1.000015	1.000015	1.000015	1.000015

Table 51 - Polarization correction factor to be applied to the responsivity values obtained with an unpolarized source instead of the linearly polarized beam.

4.12.4. Comparison with the BIPM calibrations

After corrections, including long-term drifts (see Table 5), the relative difference in the calibrations Δ is calculated for each trap as shown in Table 52.

Transfer detector	Wavelength / nm					
	476	488	514	568	633	647
	$10^4 \times$ Relative difference in trap calibration					
T3	-2.4	-1.2	-1.6	0.0	-0.1	-0.1
T13	-2.0	-1.1	-1.3	-1.0	-2.1	-0.7
P11	-1.8	0.0	-0.6	0.3	-0.6	0.2
average	-2.1	-0.8	-1.1	-0.2	-0.9	-0.2

Table 52 - Relative difference in trap calibrations $(R_{\mathrm{NMi}} - R_{\mathrm{BIPM}}) / R_{\mathrm{BIPM}}$.

The combined relative standard uncertainty of the comparison u_C is calculated using:

$$u_C^2 = u_{\mathrm{NMi}}^2 + u_{\mathrm{TRANSFER}}^2$$

where u_{NMi} is the NMi-VSL relative uncertainty,

u_{TRANSFER} is the uncertainty associated with the transfer, that is 1×10^{-4}

The calculation gives: $u_C = 2.6 \times 10^{-4}$.

4.13. ETL

4.13.1. Experimental conditions

- Cryogenic radiometer type: Radiox, from Oxford Instruments Ltd.
- Sources: He-Ne laser, Kr laser and Ar laser
- Nominal power: 400 μW
- Beam diameter ($1/e^2$): 2.2 mm
- Temperature: about 20.5 °C .

The cryogenic radiometer and the detectors to be calibrated are placed on a linear translation stage, and moved successively into the laser beam. The calibration cycle is as follows:

- an electrical-optical substitution cycle is performed with the Radiox to determine the optical power of the laser source;
- the transfer detectors are successively pushed into the beam, and their photocurrent are measured;
- a substitution cycle with the Radiox is repeated.

This cycle is repeated twenty-one to fifty times. The Brewster-angled window is isolated from the cryostat and its transmittance measured using a silicon photodiode.

4.13.2. ETL uncertainty budget

The relative standard uncertainty associated with the calibration is $u_{\mathrm{ETL}} = 4.7 \times 10^{-4}$.

Source of uncertainty	$10^4 \times$ Standard uncertainty
Radiox	
Non-equivalence electrical/optical power	0.1
Cavity absorptance	0.2
Linearity	0.6
Electrical power	0.2
Brewster Window transmittance	4.5
Scatter and diffraction	0.8
Trap detector calibration	
Trap alignment	0.6
Temperature correction	0.5
Amplifier resistance	0.2
Repeatability	0.6
Total	4.7

Table 53 - ETL uncertainty budget for the calibration of the BIPM transfer detectors.

4.13.3. Correction factors

No temperature correction correction was applied to the ETL results.

4.13.4. Comparison with the BIPM calibrations

After correction for long-term drifts (see Table 5), the relative difference in the calibrations Δ is calculated for each trap as shown in Table 54.

Transfer detector	Wavelength / nm					
	476	488	514	568	633	647
	$10^4 \times$ Relative difference in trap calibration					
T11		12.5	13.0	15.8	18.3	18.1
T12		13.8	14.0	16.2	18.1	17.3
P14		18.9	12.3	17.8	15.7	15.7
average		15.1	13.1	16.6	17.3	17.0

Table 54 - Relative difference in trap calibrations $(R_{ETL} - R_{BIPM}) / R_{BIPM}$

The combined relative standard uncertainty of the comparison u_C is calculated using:

$$u_C^2 = u_{ETL}^2 + u_{TRANSFER}^2$$

where u_{ETL} is the ETL relative uncertainty, that is 4.7×10^{-4}

$u_{TRANSFER}$ is the uncertainty associated with the transfer, that is 1×10^{-4}

The calculation gives: $u_C = 4.9 \times 10^{-4}$.

The uncertainty stated by the laboratory is large, but the relative difference in trap calibrations (up to 19 parts in 10^4) is also larger than what one would reasonably expect in such a comparison.

4.14. KRISS

4.14.1. Experimental conditions

- Cryogenic radiometer type: Radiox, from Oxford Instruments Ltd.
- Sources: He-Ne laser, Kr laser and Ar laser
- Nominal power: 300 µW to 310 µW
- Beam diameter ($1/e^2$): 2.5 mm
- Temperature: about 21.5 °C ± 0.5 °C

4.14.2. KRISS uncertainty budget

The relative standard uncertainty associated with the calibrations is $u_{KRISS} = 2 \times 10^{-4}$ (no detailed uncertainty budget).

4.14.3. Correction factors

The results were corrected for the temperature difference between the BIPM (20.5 °C) and the KRISS (21.5 °C), using the temperature coefficients given in 2.1.2.

	Wavelength / nm					
	476	488	514	568	633	647
Trap	Temperature correction factor					
T9	1.000015	1.000014	1.000013	1.000010	1.000006	1.000005
T10	1.000015	1.000014	1.000013	1.000010	1.000006	1.000005
P7	1.000026	1.000025	1.000022	1.000017	1.000010	1.000009

Table 55 - Correction factors used to correct the KRISS results for the temperature difference between the BIPM and the KRISS.

4.14.4. Comparison with the BIPM calibrations

After corrections, including long-term drifts (see Table 5), the relative difference in

the calibrations Δ is calculated for each trap as shown in Table 56.

Transfer detector	Wavelength / nm					
	476	488	514	568	633	647
	$10^4 \times$ Relative difference in trap calibration					
T9	3.1	-2.9	-3.4	3.3	-2.5	2.3
T10	2.2	-3.8	-4.8	2.5	-3.0	2.5
P7	0.4	-6.7	-7.1	1.0	-3.8	0.7
average	1.9	-4.4	-5.1	2.3	-3.1	1.8

Table 56 - Relative difference in trap calibrations $(R_{KRISS} - R_{BIPM}) / R_{BIPM}$

The combined relative standard uncertainty of the comparison u_C is calculated using:

$$u_C^2 = u_{KRISS}^2 + u_{TRANSFER}^2$$

where u_{KRISS} is the KRISS relative uncertainty, that is 2×10^{-4}

$u_{TRANSFER}$ is the uncertainty associated with the transfer, that is 1×10^{-4} for T9 and T10. Owing to the larger change in responsivity of P7 (see section 3.2.1) $u_{TRANSFER}$ was estimated to be 1.8×10^{-4}

The calculation gives: $u_C = 2.4 \times 10^{-4}$ for T9 and T10

and $u_C = 2.7 \times 10^{-4}$ for P7

4.15. IEN

4.15.1. Experimental conditions

- Cryogenic radiometer type: Radiox, from Oxford Instruments Ltd.
- Sources: He-Ne laser and Ar laser
- Nominal power: 230 µW with the He-Ne laser and 390 µW with the Ar laser
- Beam diameter ($1/e^2$): 2.5 mm
- Temperature: about 20.5 °C ± 0.5°C

4.15.2. IEN uncertainty budget

The IEN experienced some technical difficulties during the calibration procedures, both with the cryogenic radiometer itself and with the cleaning of the Brewster-angled window. These problems are reflected in the uncertainty budget, leading to a combined standard uncertainty significantly larger than the uncertainty usually achievable with such facilities.

Cryogenic radiometer Source of uncertainty	$10^4 \times$ Standard uncertainty	
	Type A	Type B
Electrical power measurement		0.9
Heating non-equivalence		0.3
Brewster window transmittance		4.0
Cavity absorption		0.1
Diffuse light		2.0
Repeatability	1.0	
Sum in quadrature	1.0	4.6

Trap detector Source of uncertainty	10^4 × Standard uncertainty	
	Type A	Type B
Current measurement		1.5
Distance effect		1.2
Diaphragm effect		1.6
Positioning of the detector		4.0
Repeatability	1.0	
Sum in quadrature	1.0	4.7

Table 57 – IEN uncertainty budget for the calibration of the BIPM transfer detectors**.**

Relative combined standard uncertainty: $u_c = 6.7 \times 10^{-4}$

4.15.3. Correction factors

No temperature correction was applied to the IEN results.

4.15.4. Comparison with the BIPM calibrations

After corrections, including long-term drifts (see Table 5), the relative difference in the calibrations Δ is calculated for each trap as shown in Table 58.

Transfer detector	Wavelength / nm					
	476	488	514	568	633	647
	10^4 × Relative difference in trap calibration					
T11		-15.3	-14.7		-0.5	
T12		-22.2	-12.8		-0.8	
P14		-15.2	-5.6		+3.3	
average		-17.6	-11.0		+0.7	

Table 58 - Relative difference in trap calibrations $(R_{IEN} - R_{BIPM}) / R_{BIPM}$

The combined relative standard uncertainty of the comparison u_C is calculated using:

$$u_C^2 = u_{IEN}^2 + u_{TRANSFER}^2$$

where u_{IEN} is the IEN relative uncertainty, that is 6.7×10^{-4}, and

$u_{TRANSFER}$ is the uncertainty associated with the transfer, that is 1×10^{-4}.

The calculation gives: $u_C = 6.8 \times 10^{-4}$

The very large differences seen at λ = 488 nm and 514 nm are probably a consequence of the technical problems mentioned in paragraph 4.15.2. After discussion with the IEN staff, it seems that at least part of the problem is related to the preparation of the laser beam; the whole experimental facility will be checked and improved in the near future.

4.16. PTB - Temperature Radiation laboratory (Berlin)

As two different laboratories from the PTB are involved in this comparison, to avoid confusion the Temperature Radiation laboratory (Berlin) will be denoted in graphs as PTB-T.

4.16.1. Experimental conditions

- Cryogenic radiometer type: vertical system, manufactured by Oxford

Instruments Ltd.; its design follows closely the first NPL cryogenic radiometer [30].

- Sources: Kr laser, Ar laser.
- Nominal power: 400 μW.
- Beam diameter: 3.2 mm

Temperature: 21.0 °C

The Radiation Thermometry Cryogenic Radiometer (RTCR) and the experimental arrangement are described elsewhere in detail [8].

4.16.2. PTB -T uncertainty budget

Source of uncertainty	$10^4 \times$ relative standard uncertainty
Measurement of the electrical power	0.3
Non-equivalence of electrical and optical power	0.5
Cavity absorptance	0.3
Transmittance of Brewster window	0.3
Scattered light	0.3
Repeatability	0.2
Combined	**0.8**

Table 59 - Contribution to the relative uncertainty of laser power calibration by electrical substitution with the cryogenic radiometer (RTCR).

Source of uncertainty	$10^4 \times$ relative standard uncertainty
Photocurrent measurement	0.2
Laser power calibration	0.8
Linearity correction	0.1
Non-uniformity	0.2
Repeatability	0.2
Combined	**0.9**

Table 60 - PTB - Radiation Thermometry laboratory: uncertainty budget for the calibration of the BIPM transfer detectors.

The PTB-T report included the contribution of the long-term stability of the transfer detectors in Table 60. As this contribution is already included elsewhere, it has been removed from the table.

4.16.3. Correction factors

The results were corrected for the small temperature difference between the BIPM and the PTB-T (0.5 °C). This correction is almost negligible.

	Wavelength / nm					
	476	488	514	568	633	647
Trap	Temperature correction factor					
T7	1.000008	1.000007	1.000006	1.000005	1.000003	1.000003
T8	1.000008	1.000007	1.000006	1.000005	1.000003	1.000003
P6	1.000013	1.000012	1.000011	1.000008	1.000003	1.000005

Table 61 - Correction factors used to correct the PTB-T results for the temperature difference between the BIPM and the PTB-T laboratory.

4.16.4. Comparison with the BIPM calibrations

After corrections, the relative difference in the calibrations Δ is calculated for each trap as shown in Table 62.

Transfer detector	Wavelength / nm					
	476	488	514	568	633	647
	$10^4 \times$ Relative difference in trap calibration					
T7	-0.6	-0.7	-0.3	-0.3		0.0
T8	-0.2	-0.5	-0.2	0.1		0.2
P6	-1.4	-1.5	-0.2	-0.6		-0.2
average	-0.7	-0.9	-0.2	-0.3		0.0

Table 62 - Relative difference in trap calibrations $(R_{\text{PTB-T}} - R_{\text{BIPM}}) / R_{\text{BIPM}}$

The combined relative standard uncertainty of the comparison u_C is calculated using:

$$u_C^2 = u_{\text{PTB-T}}^2 + u_{\text{TRANSFER}}^2$$

where $u_{\text{PTB-T}}$ is the PTB-T relative uncertainty, that is 0.9×10^{-4} , and

u_{TRANSFER} is the uncertainty associated with the transfer, that is 1×10^{-4}.

The calculation gives: $u_C = 1.3 \times 10^{-4}$.

5. Overall results

5.1. Agreement of the laboratories

As all the results from the national laboratories have been compared with the BIPM calibrations, the latter being used as a common reference (see Table 65), it is possible to calculate the difference between the results of any two participants and check if they agree within the uncertainties of the comparison. Furthermore, at each wavelength it is possible to find the maximum number of participants that agree within these uncertainties. The results of these calculations, using either the standard uncertainty or the expanded uncertainties ($k = 2$ and $k = 3$), are shown in Figure 20.

At λ = 514 nm, the common wavelength used by *all* participants, 71% of the laboratories agree within one standard uncertainty, 94% within two standard uncertainties and 100% within three standard uncertainties. Over the whole spectral range, all the calibration results agree within the expanded uncertainties (k = 3), demonstrating a satisfactory measure of the agreement of the radiometric references in the visible wavelength region, as well as the ability of the participating laboratories to transfer the values obtained using their primary standards.

Taking all the results, the dispersion calculated as the standard deviation of the relative differences is about 5×10^{-4}, but this falls to about 2.5×10^{-4} if the ETL and IEN results are excluded.

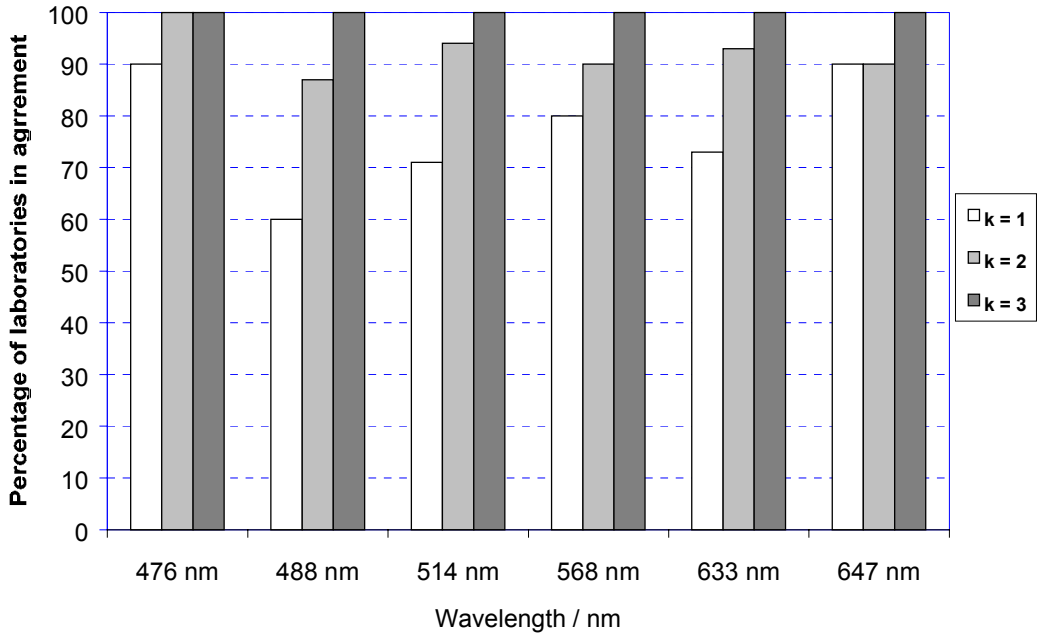

Figure 20 - Percentage of laboratories in agreement within the expanded uncertainties.

5.2. Comparison with a common reference

5.2.1. Calculation of a common reference

From all the measured differences, any common reference may be taken to display the results. Among many possibilities, are the simple mean of the differences, the median or a weighted mean.

The use of the simple mean tends to shift the reference towards the points which are significantly separated from the rest of the group.

The median is not sensitive to this effect, and it is a reasonably good candidate for the calculation of a common reference. A separate median has been calculated for each wavelength to be used as a zero baseline.

In the weighted mean, the weight w_i associated with each result x_i can be calculated from the uncertainty u_i so that:

$$w_i = \frac{\frac{1}{u_i^2}}{\sum_{i=1}^{n} \frac{1}{u_i^2}} \quad \text{and the weighted mean} \quad \overline{x_\pi} = \sum_{i=1}^{n} w_i x_i$$

Here too, a separate weighted mean has been calculated for each wavelength, using the x_i (relative difference) and u_i (uncertainty combining the standard uncertainty from each laboratory and the uncertainty associated with the transfer) summarized in Table 65.

Figure 21 shows the difference from the weighted mean $(x_i - x_\pi)$ as a function of wavelength for each participant. Numerical results are given in Table 66.

The results obtained by using either the median or the weighted mean as reference are very similar, showing that if the number of participants is large enough and if no major problem had occurred in the measurements, various statistical methods

should lead to similar results. The difference between the median and the weighted mean does not exceed 5 parts in 10^5 over the whole wavelength range (see Table 63).

Reference	Wavelength / nm					
	476	488	514	568	633	647
	$10^4 \times$ Reference value					
Weighted mean	0.1	0.6	0.7	1.0	0.5	0.9
Arithmetic mean	0.1	0.9	0.9	2.5	1.3	2.8
Median	-0.1	1.1	0.3	0.9	0.6	1.4

Table 63 – Weighted mean, arithmetic mean and median of the relative differences from the BIPM value in the calibration of the transfer detectors, as calculated from the relative differences and their associated uncertainties summarized in Table 65.

As explained in the introduction, the publication of the successive BIPM Progress Reports provided a good occasion for the participating laboratories to check their calibration procedures and in some cases to send corrected values or to take the decision to participate in a subsequent round. Figure 22 shows the relative differences before revision or new calibration. To make graphs more easily comparable, the common reference is the same as that used in Figure 21.

5.2.2. Uncertainty associated with the reference

The uncertainty associated with the weighted mean is $u_0 = \sqrt{\dfrac{1}{\sum_{i=1}^{n} \dfrac{1}{u_i^2}}}$.

The uncertainty associated with the median is based on a quantity named the 'median of the absolute deviation' (MAD):

$$\mathrm{MAD} = median\left\{\left|x_i - \tilde{m}\right|\right\}, \text{ for } i = 1...n$$

where $\tilde{m}$ is the median of the population.

The uncertainty associated with the sample median [31] is then $u(\tilde{m}) \cong \dfrac{1.9}{\sqrt{n-1}}\mathrm{MAD}$.

Reference	Wavelength / nm					
	476	488	514	568	633	647
	$10^4 \times$ uncertainty associated with the reference					
Weighted mean	0.5	0.5	0.4	0.5	0.5	0.5
Arithmetic mean	0.6	1.8	1.2	1.8	1.3	1.7
Median	1.1	1.0	0.7	0.8	0.8	0.9

Table 64 - Uncertainty associated with three possible common references.

The uncertainty u_0 associated with the weighted mean is the smallest one, approximately 0.5×10^{-4}. It is not based on the dispersion of the results, but solely on the uncertainties stated by the participants (which are in the present case combined with the uncertainty of the comparison). The agreement of the results within the combined uncertainties is an indication that these uncertainties are reasonably consistent with the actual dispersion.

In contrast, the standard deviation of the mean u_a, associated with the arithmetic mean, and $u(\tilde{m})$ (uncertainty associated with the median) are based solely on the

dispersion of the results, all of the calibrations being treated equally.

$u(\widetilde{m})$ is about 1×10^{-4} and u_a is approximately 1.5×10^{-4}. The value of u_a is given simply for information, as the arithmetic mean has not been used to calculate a common reference.

5.2.3. Choice of the CCPR reference value

For reasons explained in section 5.2.1, the arithmetic mean was discarded. The use of the median leads to robust estimations [31], which is particularly useful in the presence of outliers or when uncertainties stated by individual participants are not consistent with the results. In the absence of such problems in the present comparison, the classical weighted mean (as defined in section 5.2.1) was chosen by the CCPR during its 1999 meeting as reference value.

The uncertainty u_R associated with this reference is 5 parts in 10^5, almost constant over the whole wavelength range (see Table 64).

The uncertainty u_C associated with each individual difference from the reference value was calculated according to:

$$u_C = \sqrt{u_i^2 - u_R^2}$$

where u_i is the uncertainty combining the standard uncertainty from each laboratory and the uncertainty associated with the transfer (see section 5.2.1), the minus sign in the formula resulting from the correlation between the uncertainties u_i and u_R.

The differences from the reference value and the associated uncertainties are those listed in Table 66, plotted in Figure 21.

Laboratory	476 nm		488 nm		514 nm		568 nm		633 nm		647 nm	
	$10^4 \times \Delta$	$10^4 \times u_C$	$10^4 \times \Delta$	$10^4 \times u_C$	$10^4 \times \Delta$	$10^4 \times u_C$	$10^4 \times \Delta$	$10^4 \times u_C$	$10^4 \times \Delta$	$10^4 \times u_C$	$10^4 \times \Delta$	$10^4 \times u_C$
PTB - T	– 0.7	*1.3*	– 0.9	*1.3*	– 0.2	*1.3*	– 0.3	*1.3*			0.0	*1.3*
BNM-INM			+ 1.8	*2.0*	+ 1.1	*1.7*			+ 0.6	*1.4*		
CSIRO	+ 0.7	*1.4*	+ 2.3	*1.4*	+ 2.0	*1.4*	+ 2.1	*1.4*	+ 1.4	*1.4*	+ 1.3	*1.4*
DFM	– 2.0	*2.5*	+ 1.1	*2.5*	– 0.3	*2.5*	– 1.7	*2.5*	– 0.8	*2.5*	– 0.2	*2.5*
ETL			+ 15.1	*4.9*	+ 13.1	*4.9*	+ 16.6	*4.9*	+ 17.3	*4.9*	+ 17.0	*4.9*
HUT			+ 2.3	*2.7*	+ 1.7	*2.7*			– 0.4	*2.7*		
IEN			– 17.6	*6.8*	– 11.0	*6.8*			0.7	*6.8*		
IFA	+ 3.3	*2.2*			0.0	*2.2*	– 0.6	*2.2*	– 4.6	*2.2*	+ 2.0	*2.2*
MSL			+ 0.4	*1.2*	+ 0.3	*1.3*			+ 0.6	*1.4*		
KRISS	+ 1.9	*2.4*	– 4.4	*2.4*	– 5.1	*2.4*	+ 2.3	*2.4*	– 3.1	*2.4*	+ 1.8	*2.4*
NIST			+ 7.3	*4.5*	+ 5.9	*3.2*			+ 2.9	*4.2*		
NMi-VSL	– 2.1	*2.6*	– 0.8	*2.6*	– 1.1	*2.6*	– 0.2	*2.6*	– 0.9	*2.6*	– 0.2	*2.6*
NPL	– 0.3	*1.1*			+ 1.3	*1.1*	+ 1.9	*1.1*			+ 1.4	*1.2*
NRC	+ 1.4	*3.4*	+ 4.6	*3.4*	+ 5.3	*3.4*	+ 5.2	*3.4*	+ 4.8	*3.4*	+ 4.4	*3.4*
PTB - R			+ 3.2	*2.1*	+ 2.9	*2.9*			+ 2.5	*1.4*		
SP	– 0.8	*5.1*	– 1.4	*5.1*	– 1.0	*5.1*			– 1.3	*5.1*		
BIPM	0.0	*1.0*	0.0	*1.0*	0.0	*1.0*	0.0	*1.0*	0.0	*1.0*	0.0	*1.0*

Table 65 - Relative difference $\Delta = (R_{LAB} - R_{BIPM})/ R_{BIPM}$ in the calibration of the transfer detectors (average value obtained from three transfer detectors per laboratory) calculated at each wavelength. The uncertainty u_c combines the relative standard uncertainties from each laboratory and the uncertainty associated with the transfer. Values are expressed in parts in 10^4. The acronyms PTB-R and PTB-T stand for PTB-Radiometry laboratory, and PTB-Temperature Radiation laboratory respectively.

Laboratory	476 nm		488 nm		514 nm		568 nm		633 nm		647 nm	
	$10^4 \times \Delta_{Ref}$	$10^4 \times u_C$	$10^4 \times \Delta_{Ref}$	$10^4 \times u_C$	$10^4 \times \Delta_{Ref}$	$10^4 \times u_C$	$10^4 \times \Delta_{Ref}$	$10^4 \times u_C$	$10^4 \times \Delta_{Ref}$	$10^4 \times u_C$	$10^4 \times \Delta_{Ref}$	$10^4 \times u_C$
PTB - T	– 0.8	*1.2*	– 1.5	*1.3*	– 0.9	*1.3*	– 1.3	*1.2*			– 0.9	*1.2*
BNM-INM			+ 1.1	*1.9*	+ 0.5	*1.6*			+ 0.1	*1.3*		
CSIRO	+ 0.7	*1.3*	+ 1.7	*1.3*	+ 1.3	*1.3*	+ 1.1	*1.3*	+ 0.9	*1.3*	+ 0.4	*1.3*
DFM	– 2.0	*2.5*	+ 0.4	*2.5*	– 1.0	*2.5*	– 2.7	*2.5*	– 1.3	*2.5*	– 1.1	*2.5*
ETL			+ 14.4	*4.9*	+ 12.5	*4.9*	+ 15.6	*4.9*	+ 16.8	*4.9*	+ 16.1	*4.9*
HUT			+ 1.6	*2.6*	+ 1.1	*2.7*			– 0.9	*2.6*		
IEN			– 18.2	*6.8*	– 11.7	*6.8*			+ 0.2	*6.8*		
IFA	+ 3.3	*2.2*			– 0.7	*2.2*	– 1.6	*2.2*	– 5.1	*2.2*	+ 1.0	*2.2*
MSL			– 0.2	*1.0*	– 0.3	*1.2*			+ 0.1	*1.3*		
KRISS	+ 1.8	*2.3*	– 5.1	*2.3*	– 5.8	*2.3*	+ 1.3	*2.3*	– 3.6	*2.3*	+ 0.9	*2.3*
NIST			+ 6.7	*4.5*	+ 5.2	*3.2*			+ 2.4	*4.1*		
NMi-VSL	– 2.1	*2.5*	– 1.4	*2.6*	– 1.8	*2.6*	– 1.2	*2.5*	– 1.4	*2.6*	– 1.2	*2.5*
NPL	– 0.4	*1.0*			+ 0.7	*1.0*	+ 0.9	*0.9*			+ 0.5	*1.0*
NRC	+ 1.4	*3.4*	+ 4.0	*3.4*	+ 4.7	*3.4*	+ 4.2	*3.4*	+ 4.3	*3.4*	+ 3.4	*3.4*
PTB - R			+ 2.6	*2.1*	+ 2.2	*2.8*			+ 2.0	*1.3*		
SP	– 0.9	*5.1*	– 2.0	*5.1*	– 1.7	*5.1*			– 1.8	*5.1*		
BIPM	– 0.1	*0.9*	– 0.6	*0.9*	– 0.7	*0.9*	– 1.0	*0.9*	– 0.5	*0.9*	– 0.9	*0.9*

Table 66 - Difference Δ_{Ref} from the CCPR Reference value (weighted mean of the relative differences) in the calibration of the transfer detectors calculated at each wavelength. The uncertainty u_c combines the relative standard uncertainties from each laboratory, the uncertainty associated with the transfer and the uncertainty associated with the reference value. Values are expressed in parts in 10^4. The acronyms PTB-R and PTB-T stand for PTB-Radiometry laboratory, and PTB-Temperature Radiation laboratory respectively.
The uncertainty associated with the reference value is 5 parts in 10^5.

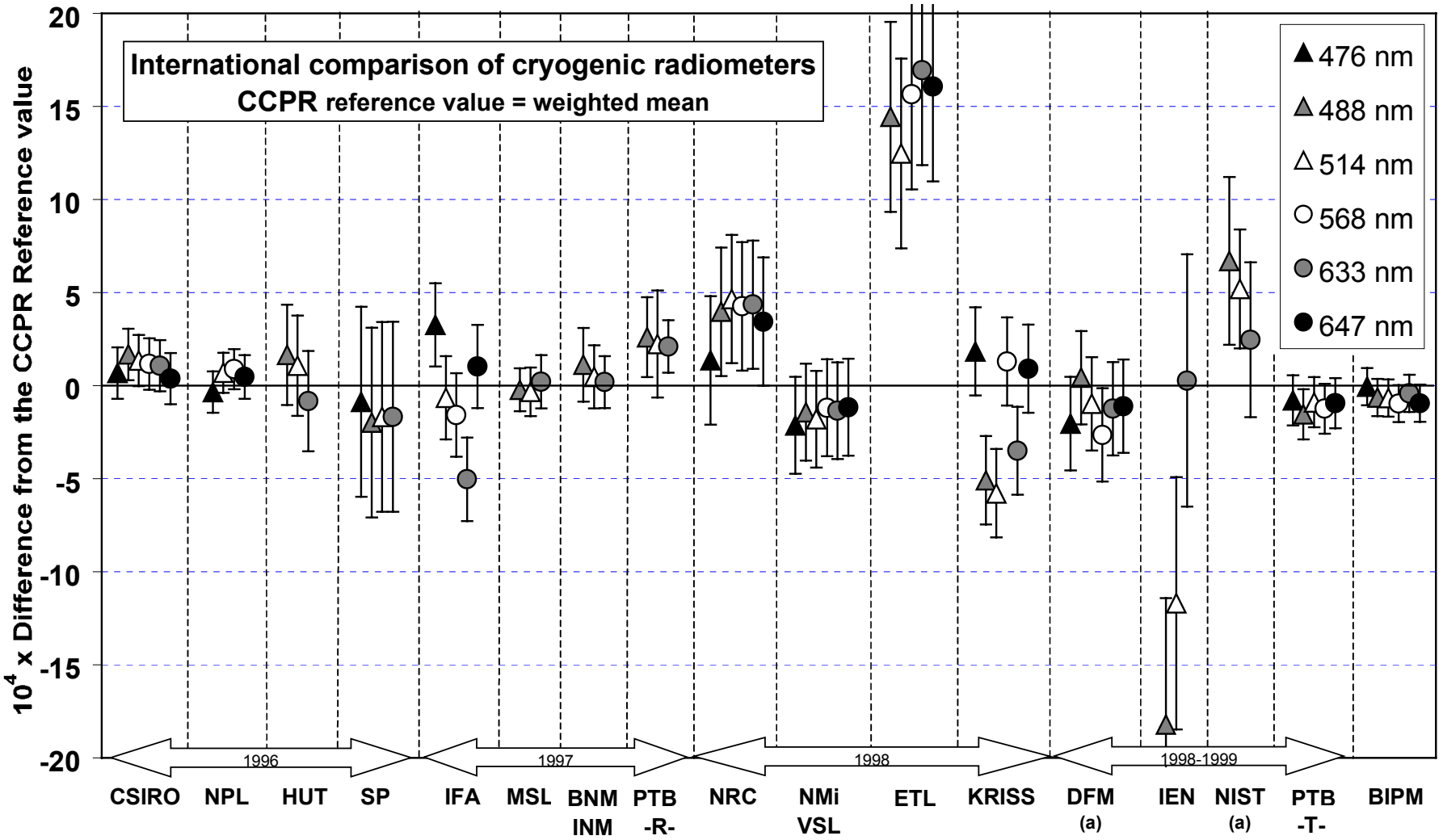

Figure 21 - Relative difference in the calibration of the transfer detectors (average value obtained from three transfer detectors per laboratory). The CCPR Reference value (zero line) is the weighted mean of the relative differences (R_{LAB} - R_{BIPM})/ R_{BIPM} calculated at each wavelength. The uncertainty bars combine the relative standard uncertainties from each laboratory and the uncertainty associated with the transfer. The acronyms PTB-R and PTB-T stand for PTB-Radiometry laboratory, and PTB-Temperature Radiation laboratory, respectively. Laboratories marked with a (a) have also participated in a previous round. The uncertainty associated with the reference is about 5 parts in 10^5.

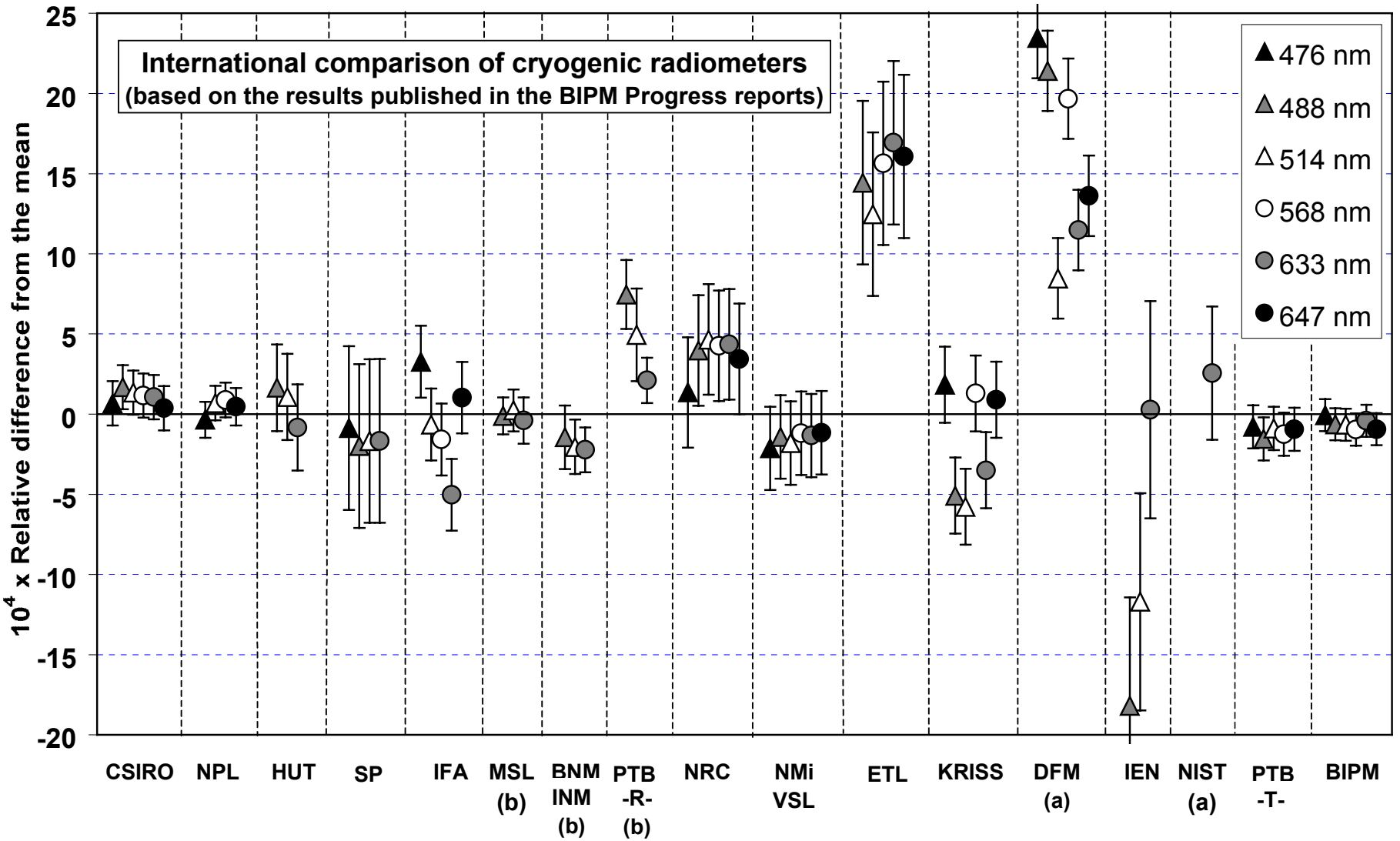

Figure 22 - Relative difference in the calibration of the transfer detectors. The zero line (CCPR reference value) and the uncertainty bars are the same as those used in Figure 21. The acronyms PTB-R and PTB-T stand for PTB-Radiometry laboratory, and PTB-Temperature Radiation laboratory, respectively. Results marked with a (a) correspond to results published in the BIPM Progress reports after the first participation of the laboratory (which later repeated its measurements). Results marked with a (b) correspond to values published in the BIPM Progress reports, before revision by the participating laboratory.

5.3. Link with previous direct comparisons

In the experiments reported here, the uncertainties associated with the experimental conditions, or with the transfer, are of the same order of magnitude as the uncertainties associated with the radiometers (or even larger). It is therefore difficult to estimate the specific contribution made by the cryogenic radiometers, but it is interesting to link the present results to previous direct comparisons. The effects of a possible contribution of the radiometers can be estimated the following way:

By definition, the measured responsivity is $R = \dfrac{I_{\mathrm{PHOT}}}{P_{\mathrm{OPT}}}$

where I_{PHOT} is the photocurrent and P_{OPT} the optical power measured by the radiometer. If P_{OPT} is larger than the actual optical power, the measured responsivity will be smaller than expected, and vice-versa.

Denoting by R_{A} and R_{B}, respectively, the calibration results of a single trap from laboratories A and B, the inequality $R_{\mathrm{A}} > R_{\mathrm{B}}$ can be interpreted as meaning that if the radiometers A and B were placed on the same translation stage to measure the optical power of the same constant source, the optical power measured by radiometer B would be larger than that measured by radiometer A. This observation makes it possible to plot some of the present results on the same graph as results from previous direct comparisons.

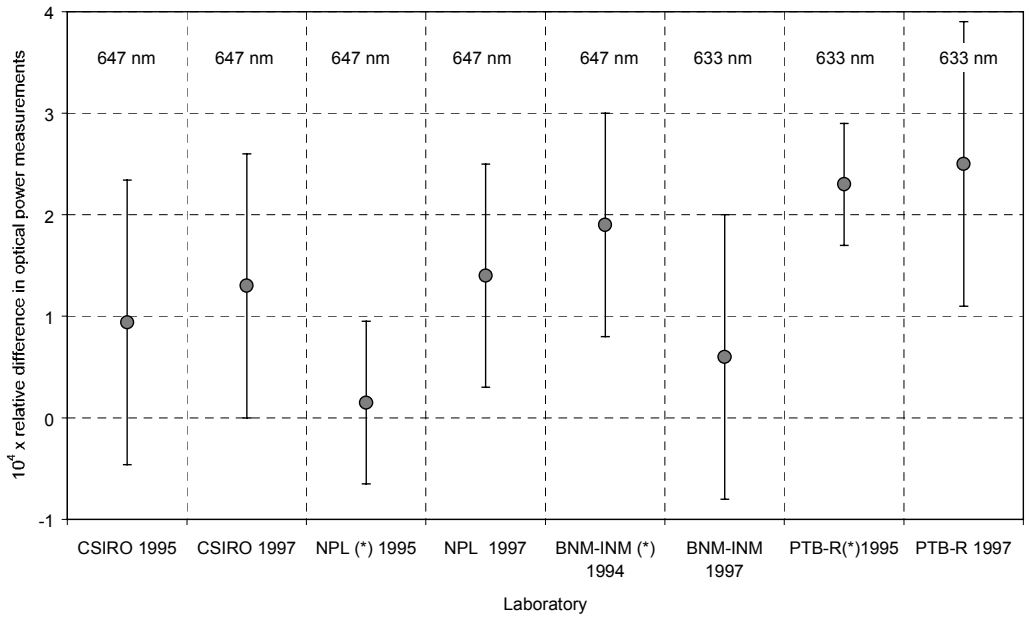

Figure 23 - Comparison of the BIPM cryogenic radiometer with other laboratories: previous measurements and results from this comparison. Results marked with a (*) are direct comparisons. The zero line represents the BIPM used as a common reference. The uncertainty bars represent the relative combined standard uncertainties. The acronym PTB-R stands for PTB Radiometry laboratory (Braunschweig).

The results of direct previous comparisons of cryogenic radiometers are presented by calculating the relative difference as:

$$\Delta_{\mathrm{direct}} = \frac{P_{\mathrm{BIPM}} - P_{\mathrm{LabA}}}{P_{\mathrm{BIPM}}}$$

where P_{BIPM} and P_{labA} are the optical powers of a same constant source as measured by the cryogenic radiometers from BIPM and laboratory A respectively.
This expression is equivalent to the expression:

$\Delta = (R_A - R_{BIPM}) / R_{BIPM}$ used for the present results.

The relative differences determined from direct and indirect comparisons are shown on Figure 23.

6. Conclusions

The overall agreement of the calibrations within the expanded uncertainties confirms the excellent agreement of cryogenic radiometers of various types and origins: horizontal and cooled by liquid helium, horizontal and mechanically cooled, vertical but of different shapes, laser-based or monochromator-based arrangements.

Most of the results lie within ± 3 parts in 10^4 (the standard uncertainty associated with the transfer being 1 part in 10^4), and previous direct or indirect comparisons are confirmed.

This demonstrates both close agreement of the radiometric references in the visible wavelength region, and the ability of participating laboratories to transfer the values obtained using their primary standards.

Transfer detectors allow highly accurate comparisons, if used under carefully controlled experimental conditions: preliminary experiments and results from the national laboratories show the importance of parameters such as beam diameter (i.e. irradiance level), beam polarization and protection against dust contamination. More generally, the quality of the beam preparation has shown to be crucial in high-accuracy cryogenic radiometry.

Thanks to their good stability, uniformity and low temperature coefficient, the trap detectors constructed with S1337 photodiodes are confirmed as appropriate transfer detectors, except when high irradiance levels are required. Trap detectors assembled with S1227 photodiodes can be a good alternative in such a case.

This comparison also allowed several laboratories to improve their experimental arrangement or to eliminate previously undetected errors.

The pilot laboratory wishes to thank all the participants for their cooperation which allowed the comparison to be completed on time.

7. APPENDIX

7.1. Document sent to the participating laboratories

The following document was sent to the participating laboratories together with the detectors to be calibrated.

Experimental parameters

All measurements at the BIPM were made with the following parameters:

beam-diameter: 2 mm to 2.5 mm ($1/e^2$ diameter)
radiant intensity: 400 μW (typical)
temperature: 20.5 °C

Participants are not obliged to use identical parameters but must communicate the values used to the BIPM to allow for the calculation of correction factors. The use of parameters as close as possible to these would reduce the uncertainties of the comparison.
If the beam diameter is smaller than 2 mm ($1/e^2$), then the radiant intensity should be decreased, so as to avoid non-linearity effects in the detector responsivity.

All the detectors were calibrated at the BIPM at all the wavelengths proposed for the comparison, namely:

476.2 nm (Kr line) - 488.0 nm (Ar line) - 514.5 nm (Ar line) - 568.2 nm (Kr line)- 632.8 nm (He-Ne line) - 647.1 nm (Kr line).

Participants should calibrate the detectors at least at three wavelengths on this list. The argon line at 514.5 nm is the proposed common wavelength and should be used if possible.

Alignment procedures

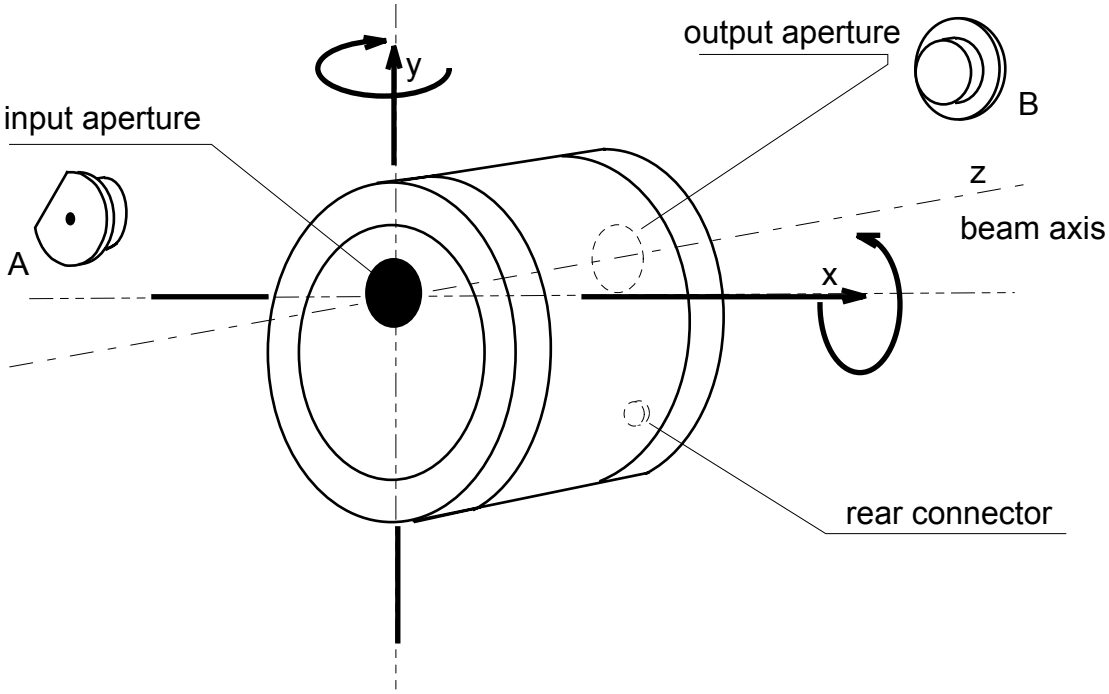

Figure 1. Alignment procedure for transmission traps.
A: input aperture alignment device (brass)
B: output aperture alignment device (semi transparent)

Alignment procedure for transmission traps
(see Fig. 1)

a) remove completely the two rotatable dust caps
b) insert the alignment device A (made of brass, with a flat side) in the input aperture
c) translate the trap along the x and y axis to align the central hole in the beam
d) insert the semi-transparent alignment device B in the output hole
e) rotate the trap about the x and y axis so that the output beam hits the center of B
f) repeat steps 'c' to 'e' until the input beam and the output beam are centred in the input and output hole respectively.

Alignment procedure for the reflection trap.
(see Fig. 2)

a) remove the whole plastic dust cap
b) insert the alignment device C in the input hole
c) translate the trap along the x and y axis to align the central hole in the beam
d) rotate the trap about the x and y axis so that the weak residual reflected beam is collinear with the input beam.
e) repeat steps 'b' to 'd' to check both the position and the orientation.

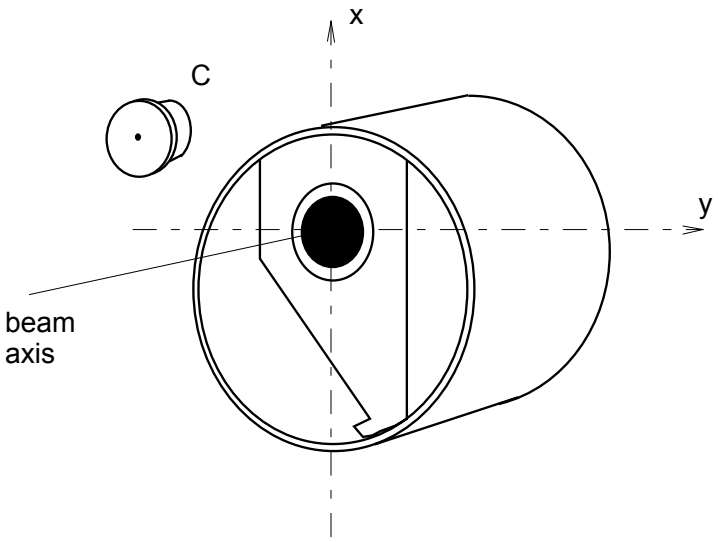

Figure 2. Alignment procedure for the reflection trap. C: alignment device (brass)

Orientation with respect to the direction of polarisation of the input beam.

Trap detectors show a residual sensitivity to the state of polarisation of the beam. An orientation with respect to the direction of polarisation has been chosen arbitrarily, and the traps have to be calibrated and used always oriented the same way.

Transmission traps:
The line joining the center of the input face and the center of the input hole has to be parallel to the direction of vibration of the electrical vector (see Fig. 3-a).

Reflection trap:
The direction of vibration has to be parallel to the flat part on the right hand side of the mechanical mounting (reference side), as shown on Fig.3-b.

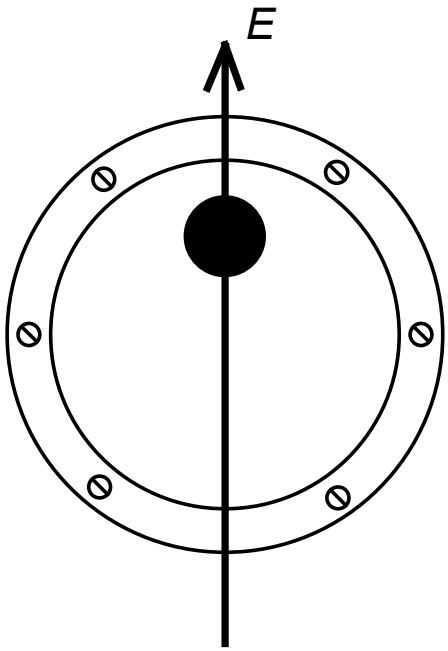

Figure 3-a. Orientation of the transmission traps with respect to the direction of polarization of the beam.

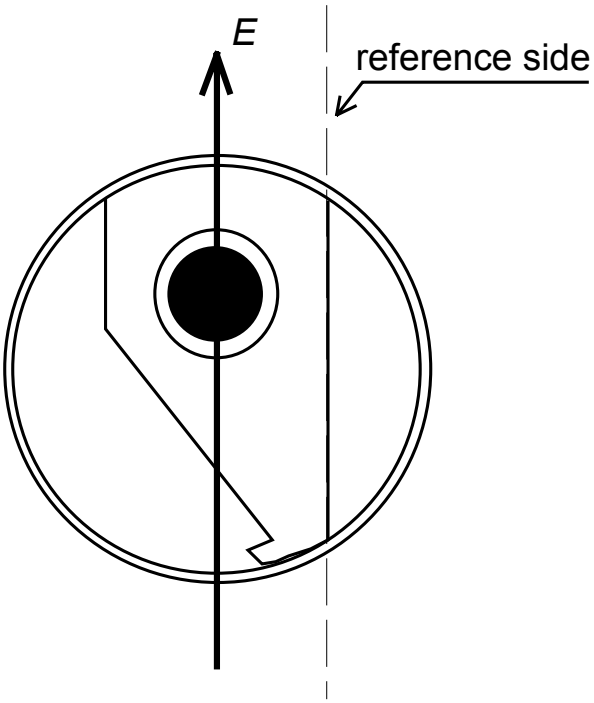

Figure 3-b. Orientation of the reflection traps with respect to the direction of polarization of the beam.

7.2. List of figures

7.3. List of tables

7.4. List of acronyms

BNM-INM	Bureau National de Métrologie – Institut National de Métrologie, Paris, France.
CSIRO	Commonwealth Scientific and Industrial Research Organization, Lindfield, Australia.
DFM	Danish Institute of Fundamental Metrology, Lyngby, Denmark.
ETL	Electrotechnical Laboratory, Tsukuba, Japan.
HUT	Helsinki University of Technology, Espoo, Finland.
IFA	Instituto de Fisica Aplicada, Madrid, Spain.
KRISS	Korea Research Institute of Standards and Science, Taejon, Rep.of Korea.
NIM	National Institute of Metrology, Beijing, P. Rep. of China.
NIST	National Institute of Standards and Technology, Gaithersburg, USA.
NMi-VSL	Nederlands Meetinstituut, Delft, The Netherlands.
NPL	National Physical Laboratory, Teddington, United Kingdom.
NRC	National Research Council, Ottawa, Canada.
PTB	Physikalisch-Technische Bundesanstalt, Braunschweig and Berlin, Germany.
MSL	Measurement Standards Laboratory - Industrial Research Limited Lower Hutt, New Zealand.
SP	Statens Provningsanstalt, Boras, Sweden.

8. REFERENCES

1 Comité Consultatif de Photométrie et Radiométrie, Report of the 13th Meeting, 1994, BIPM publication.

2 R. Köhler, R. Goebel, R. Pello, O. Touayar, J. Bastie, First results of measurements with the BIPM cryogenic radiometer and comparison with the INM cryogenic radiometer , Proc. of the NEWRAD conference, Berlin, 1994, *Metrologia*, 1996, **32**, 551-555

3 R. Goebel, R. Pello, R. Köhler, P. Haycocks and N. Fox, Comparison of the BIPM cryogenic radiometer with a mechanically cooled cryogenic radiometer from the NPL, *Metrologia,* 1996, **33**, 177-179.

4 N.P. Fox, J. Martin, Comparison of two cryogenic radiometers by determining the absolute spectral responsivity of silicon photodiodes with an uncertainty of 0.02%, *App. Opt*, 1990, **29**, 4686-4693.

5 N.P. Fox , Trap detectors and their properties, *Metrologia*, 1991, **28**, 197-202.

6 J. L. Gardner, Transmission trap detectors, *Appl. Opt*., 1994, **33**, 5914-5918.

7 R. Köhler, R. Goebel, R. Pello, Report on the international comparison of spectral responsivity of silicon detectors, 1994, Rapport BIPM 94-9.

8 Fu Lei and J. Fisher, Characterization of Photodiodes in the UV And Visible Spectral Range Based on Cryogenic Radiometry, *Metrologia*, 1993, **30**, 297-303.

9 T. Kübarsepp, P. Kärhä., E. Ikonen, Characterization of a polarization-independent transmission trap detector, *Appl. Opt*., 1997, **36**, 2807-2812.

10 J. Campos, P. Corredera, A. Pons, A. Corrons, J.L. Fontecha, Reflectance dependencies of silicon trap detectors, *Metrologia*, 1998, **35**, 455-460.

11 R. Goebel, S. Yilmaz and R. Pello, Polarization dependence of trap detectors, *Metrologia*, 1996, **33**, 207-213.

12 K.D. Stock, S. Morozova, L. Liedquist and H. Hofer, Nonlinearity of the quantum efficiency of Si reflection trap detectors at 633 nm, *Metrologia*, 1998, **35**, 451-454.

13 R. Goebel and M. Stock, Non linearity and polarization effects in silicon trap detectors, *Metrologia*, 1998, **35**, 413-418.

14 T. Kübarsepp, A. Haapalina, P. Kärhä and E. Ikonen, Nonlinearity measurements of silicon photodetectors, *Appl. Opt*, 1998, **37**, 2716-2722.

15 J. Metzdorf, W. Möller, T. Wittchen and D. Hünerhoff, Principle and Application of Differential Spectroradiometry, *Metrologia*, **28**, 1991, 247-250.

16 J. Fischer and Lei Fu, Photodiode nonlinearity measurement with an intensity stabilized laser as a radiation source*, Appl. Opt*., 1993, **32**, 4187-4190.

17 R. Köhler, R. Goebel, R. Pello and J. Bonhoure, Effects of humidity and cleaning on the sensitivity of Si photodiodes, *Metrologia,* 1991, **28**, 211-215.

18 R. Goebel, S. Yilmaz and R. Köhler, Stability under vacuum of silicon trap detectors and their use as transfer instruments in cryogenic radiometry, *Appl Opt*, 1996, **35**, 4404-4407.

19 R. Goebel, R. Köhler and R. Pello, Experimental Procedures for the comparison of cryogenic radiometers at the highest accuracy, *Metrologia,* 1996, **33**, 549-554.

20 D.J. Butler, R. Köhler, G.W. Forbes, Diffraction effects in the radiometry of coherent beams, *Applied Optics*, 1996, **35**, 2162-2166.

21 O. Touayar, B. Rougié, J.M. Coutin and J. Bastie, Measurement of the reflectance of the INM cryogenic radiometer cavity at several wavelengths, *Metrologia*, 1998, **35**, 387-391.

22 K.D. Stock, and H. Hofer, PTB primary standard for optical radiant power: transfer-optimized facility in the clean-room center, Metrologia, 1995/1996, **32**, 545-549.

23 Stock K.D., Hofer H., Present State of the PTB Primary Standard for Radiant Power Based on Cryogenic Radiometry, *Metrologia*, 1993, **30**, 291-296

24 Goebel R., Pello R., Stock K.D., Hofer H., Short Communication: Direct comparison of cryogenic radiometers from the BIPM and the PTB, *Metrologia*, 1997, **34**, 257-259.

25 K.M. Nield, J.F. Clare, J.D. Hamlin and A. Bittar, Calibration of a trap detector against a cryogenic radiometer, *Metrologia*, 1998, **35**, 581-586.

26 Boivin L.P. and Gibb K., Monochromator-based cryogenic radiometry at the NRC, *Metrologia*, 1995/1996, **32**, 565-570.

27 L.P. Boivin, Measurements using two types of transfer radiometer developed for a monochromator-based cryogenic radiometer facility, *Metrologia*, 1998, **35**, 363-368.

28 Handbook of lasers, CRC Press.

29 C.A. Schrama, R. Bosma, K. Gibb, H. Reyn and P. Bloembergen, Comparison of monochromator-based and laser-based cryogenic radiometry, *Metrologia*, 1998, **35**, 431-435.

30 J.E. Martin, N.P. Fox, P.J. Key, *Metrologia*, 1985, **21**,147-155.

31 J.W. Müller, Possible advantages of a robust evaluation of comparisons, *BIPM report* BIPM-95/2.